Environ Geol (2007) 52:225–249
DOI 10.1007/s00254-006-0585-6

ORIGINAL ARTICLE

Salt and ice crystallisation in porous sandstones

Joerg Ruedrich · Siegfried Siegesmund

Received: 12 November 2006 / Accepted: 14 November 2006 / Published online: 19 December 2006

Abstract Salt and ice crystallisation in the pore spaces causes major physical damage to natural building stones. The damaging effect of these processes can be traced back to physically induced stress inside of the rock while crystallizing. The increasing scientific research done during the past century has shown that there are numerous parameters that have an influence on the weathering resulting from these processes. However, the working mechanisms of the stress development within the rock and its material dependency are still subject to discussion. This article gives an overview of salt and ice weathering. Additionally, laboratory results of various sandstones examined are presented. Salt crystallisation tests and freeze/thaw tests were done to obtain information about how crystallisation weathering depends on material characteristics such as pore space, water transportation, and mechanical features. Simultaneous measuring of the length alternating during the salt and ice crystallisation has revealed detailed information on the development of crystal in the pore spaces as well as the development of stress. These findings can help to understand the damaging mechanisms.

Keywords Salt and ice crystallisation · Sandstone · Physical weathering processes · Length change behaviour · Stone deterioration

J. Ruedrich (✉) · S. Siegesmund
Geoscience Center University Goettingen,
Goldschmidtstr. 3, 37077 Goettingen, Germany
e-mail: jruedri@gwdg.de

Introduction

In many cases damage to porous building stones is caused by salt and ice crystallisation within the pores. Despite the existing abundance of observations, laboratory results, and theoretical considerations on this subject, the actual damaging process is still being discussed. Evidently, that is because the synergistically damaging mechanisms make the buildings highly complex. Moreover, the quality of natural stone is difficult to determine because of its heterogeneous character and frequent anisotropy of the petrophysical properties. In order to gain more knowledge of the weathering process that salt and ice crystallisation cause, laboratory experiments are needed to test the damaging dynamics as well as the effective forces that are related to the heterogeneity and the anisotropy of natural stone.

The aim of the present article is to give a general overview of the state of knowledge about the weathering that results from salt and ice crystallisation in the pore spaces of natural building stones. Supplementary results of laboratory examinations of the salt and frost weathering of sandstones are given as an example. Twelve sandstone types of varying mineralogical compositions and different fabric properties were selected: Cotta, Ruethen, Bentheim, Velpke, Ostlutter, Obernkirchen, Hockeln, Heersum, Ibbenbueren, Schoetmar, Karlshafen, and Barkhausen (all from quarries located in Germany). The studies focused on the fabric-controlled effects on salt and ice weathering. Comprehensive analyses of the fabric as well as the petrophysical characteristics were combined with common weathering tests and measurements of the length change during the salt and ice crystallisation.

First, the material properties will be determined, which includes microscopic examinations of the rock fabric (mineralogical content, grain size, sorting, grain shape, etc.) and the petrophysical properties (porosity, pore radii distribution, capillary water absorption, water vapour diffusion, critical water content, tensile strength, and compressional wave velocity). Second, the theoretical background as well as the weathering investigations of both salt and ice weathering will be presented.

Rocks investigated

Rock fabrics

The specific rock fabric of sandstones in terms of size, sorting, roundness of detrital grains, grain contacts, and cement properties significantly controls the petrophysical properties as well as the material behaviour during the weathering. The fabric is the result of the complex formation during sedimentation, compaction, diagenesis, and alteration. The selected sandstones derive from different geological periods between the carboniferous and the cretaceous and represent diverse lithotypes. They are characterized by a large variety of fabric elements. In order to describe the quality of the different grain parameters (e.g. mineralogical composition, properties of detrital, and authigenic components), fabric analyses were performed in polarized light on standard thin sections. To determine the grain size and preferred grain boundary orientation, quantitative image analyses were applied.

In order to take the directional dependency of the fabric parameters into account, the investigations were carried out on specimens from three mutually perpendicular directions. A reference coordinate system for the investigations, with respect to the macroscopically visible elements of foliation and lineation, was chosen (X, Y, Z). The XY-plane marks sedimentary bedding. An arbitrary coordinate system was defined if the specimens did not show any macroscopically visible fabric elements. A compilation of the main fabric parameters as well as the petrographic features is given in Table 1.

The main components of the investigated sandstones are detrital quartz grains, followed by some feldspar. The sandstones from Velpke, Bentheim and Obernkirchen represent extensive pure quartz sandstone with a small amount of kaolinite. Their ochre yellow colour is derived from iron oxide and hydroxide. The other investigated sandstones are characterized by a varying content of clay minerals and micas (cf. Table 1). The material of Ostlutter and Ruethen is green sandstone, with glauconite being responsible for that colour. In contrast to that, the green colour of the Barkhausen sandstone results from a high chlorite concentration. The Karlshafen sample shows some hematite, which made it red in colour.

A basic descriptive element of sandstone is the grain size because it affects the pore space properties, e.g. the pore size distribution. The samples investigated here vary in detrital grain size between 50 and 600 μm (Table 1). The most fine-grained sample derived from Heersum. With a grain size from 50 to 100 μm it represents a transition type between silt and sandstone. The most coarse-grained sample is the one from Ostlutter. Its grain size varies between 100 and 600 μm.

The samples also differ fundamentally as far as the sorting is concerned. Whereas the samples from Bentheim, Velpke, and Obernkirchen are well sorted and represent more or less mutual beach sediments,

Table 1 Fabric properties of the investigated sandstone types

Sandstone type	Abbreviation	Detritus				Authigen minerals	
		Grain size (μm)	Sorting	Roundness	Main phases	Clay content	Cements
Cotta	CO	100–200	Well	Rounded	Qz, Fsp, Mc, Clay	Low	Qz, Clay
Ruethen	RU	100–400	Moderate	Well rounded	Qz, Fsp	Low	Qz
Bentheim	BE	100–300	Moderate	Rounded	Qz, Fsp	Very low	Qz
Velpke	VE	100–200	Well	Angular	Qz	Very low	Qz
Ostlutter	OL	100–600	Bimodal	Well rounded/angular	Qz	Low	Qz
Obernkirchen	OK	100–200	Well	Angular	Qz, Fsp	Very low	Qz
Hockeln	HO	100–200	Poorly	Well rounded	Qz, Fsp	Very low	Qz, Clay
Heersum	HE	50–200	Moderate	Rounded	Qz, Fsp, Mc	High	Qz, Clay
Ibbenbueren	IB	200–400	Well	Rounded	Qz, Fsp, Mc	Low	Qz, Clay
Schoetmar	SC	100–200	Moderate	Angular	Qz, Fsp, Clay	High	Fsp, Qz, Clay
Karlshafen	KA	100–300	Moderate	Angular	Qz, Fsp, Mc	Low	Qz, Fsp, Clay
Barkhausen	BH	50–200	Well	Angular	Qz, Fsp, Mc	High	Qz, Fsp, Clay

Qz quartz, *Fsp* feldspar, *Mc* mica

the other sandstone types show moderate to pure sorting (Fig. 1). An exception is the Ostlutter sandstone, which shows a bimodal grain size distribution. The main fraction's grain size is between 100 and 300 μm, whereas the subordinate fraction shows grain diameters of 400–600 μm.

The roundness of detrital grains has a significant influence on the pore geometry of sandstones. Regarding the investigated samples and the respective sandstones, the findings show that their roundness varies a lot. The samples from Bentheim and Velpke have almost round grain shapes, whereas the other sandstones' grains show mostly sub-angular to angular geometries (Table 1). The Ostlutter sandstone with its bimodal grain size distribution differs from these. Its smaller grain fraction shows mostly sub-angular geometries, whereas the grains of the larger fraction are preferably well rounded (Fig. 1b). This can be taken as evidence for two geological source areas.

Some of the investigated samples show oval shapes of the clastic sand grains with a preferred orientation of long axis parallel to the bedding. This fabric characteristic is well developed for the sandstone from Cotta. The orientation of grain boundaries is exemplarily shown in Fig. 2 for the Bentheim and Cotta sandstone. Whereas the Bentheim sandstone show more or less equal distribution of the grain boundary orientation, the Cotta sandstone is characterized by a preferred orientation of boundaries perpendicular to the *Z*-direction.

All the investigated sandstones are more or less grain supported. The contacts between the detrital grains developed mostly in a planar and subordinately concavo-convex way. Only a few sutured contacts were found in the Karlshafen sandstone. All the samples show quartz cements as a syntaxial grain overgrowth, whereas the intensity and frequency differ. The Schoetmar and Barkhausen sandstone additionally exhibit a large amount of feldspar cements. The clay content is only high in the samples from Ibbenbueren, Schoetmar, Barkhausen, and Karlshafen, but it can be expected that it will not significantly contribute to the material cohesion.

Petrophysical properties

Their mineralogical composition and fabric determine the petrophysical properties of the rocks. Due to the pronounced fabric differences of the investigated rocks, their petrophysical properties also vary greatly.

To characterize the total accessible porosity, measurements of buoyancy weighting were performed. The samples were mounted in a basket attached under a scale and the dry mass, the water-saturated mass, and the mass immersed in water were determined. The investigated samples show a wide range of porosity, which more or less covers the whole spectrum expected for sandstones and varies between 3.4 and 25.7% (Table 2). The sandstones can be subdivided in three porosity groups: low (<10%), medium (10–20%), and high porosity (>20%). The latter group contains the sandstones from Cotta, Bentheim, Velpke, Ruethen, and Ostlutter. The samples from Obernkirchen, Hockeln, Heersum, and Ibbenbueren show medium porosity, whereas the Schoetmar, Karlshafen, and Barkhausen sandstones are of low porosity.

The pore size distribution of the samples was determined by using mercury porosimetry (cf. Brakel

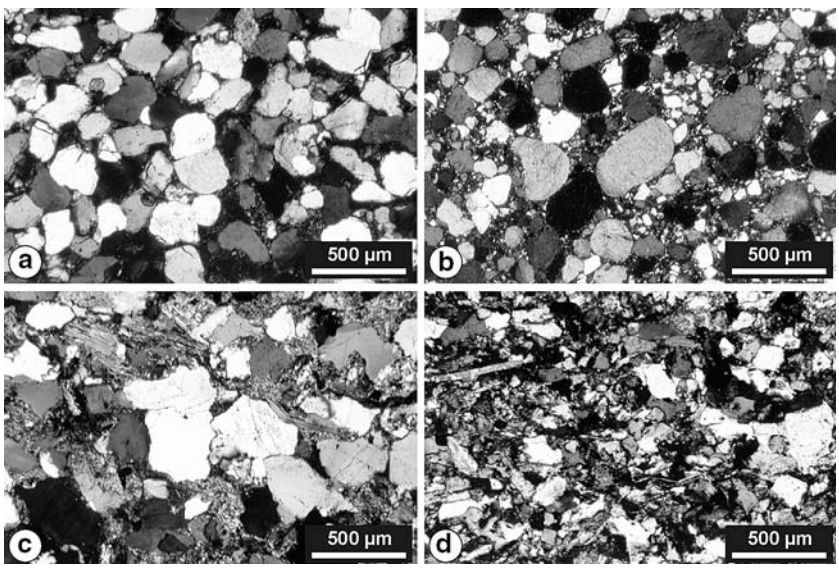

Fig. 1 Thin section photomicrographs (crossed polarisers): **a** well rounded quartz grains of Bentheim sandstone, **b** bimodal grain size distribution of the Ostlutter sandstone, **c** angular quartz grains and heterogeneous compostion of the Schoetmar sandstone and **d** fine grained micro fabric dominated by quartz grains of the Karlshafen sandstone

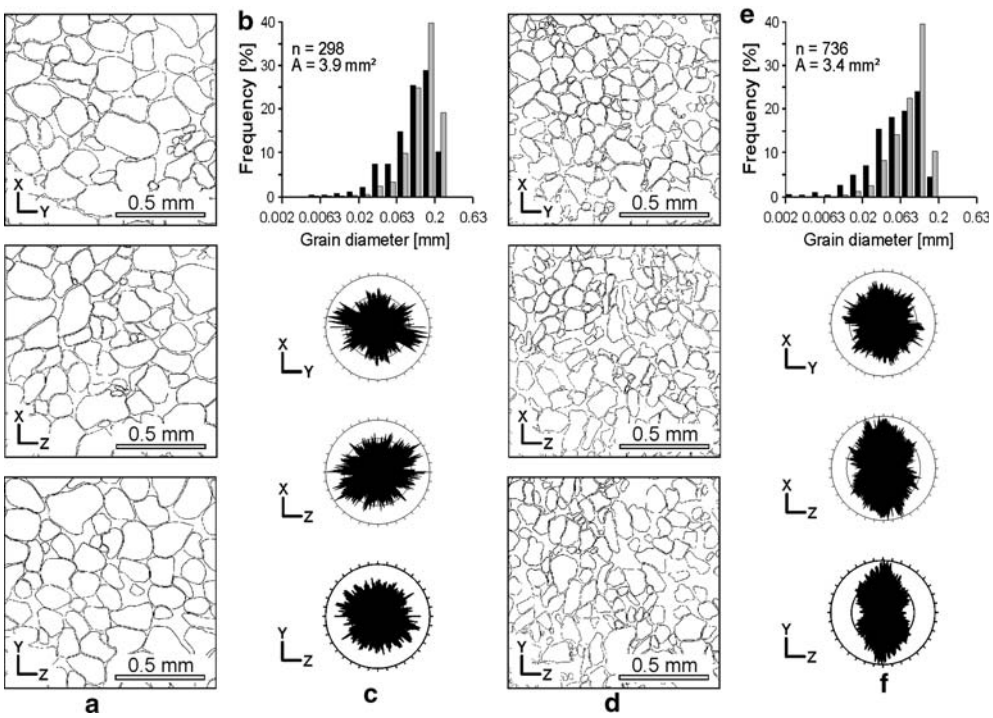

Fig. 2 Detrital grain characteristics determined by image analyses for the Bentheim (**a**–**c**) and Cotta sandstone (**d**–**f**): **a**, **d** line drawings of detrital grains of the *XY*, *XZ*, and *YZ* plane, **b**, **e** grain diameter frequency (*A* analyzed area; *n* number of grains) and **c**, **f** grain boundary orientation in the *XY*, *XZ*, and *YZ* plane

Table 2 Pore space properties of the investigated sandstone types

Sandstone type	Porosity	Pore radii type	Average pore radius	Pore radii distribution (%)				
				0.001–0.01	0.01–0.1	0.1–1	1–10	>10
Cotta	25.7	C	1.73	2.8	6.9	23.9	54.7	11.7
Ruethen	25.6	C	3.20	7.6	11.7	4.1	12.9	63.7
Bentheim	24.8	A	9.15	2.8	3.2	2.7	10.3	81.1
Velpke	24.7	A	7.49	1.7	3.1	3.3	32.2	59.7
Ostlutter	20.8	C	9.59	2.7	3.2	2.0	15.7	76.4
Obernkirchen	17.7	B	0.97	1.9	8.1	20.9	66.7	2.4
Hockeln	15.4	C	1.78	3.8	12.2	7.9	66.7	9.4
Heersum	15.1	B	0.20	5.2	16.4	74.5	3.0	0.9
Ibbenbueren	10.9	B	0.18	5.9	24.7	59.6	2.3	7.5
Schoetmar	8.1	C	0.07	20.2	38.1	32.3	5.4	4.0
Karlshafen	5.1	B	0.06	8.4	48.8	42.3	0.5	0.0
Barkhausen	3.4	C	0.04	29.0	57.8	3.2	2.1	7.9

et al. 1981). For the investigated sandstones the pore size distribution pattern can be distinguished in three types (Fig. 3). Type A shows a narrow spaced pore radii maximum, and is therefore more or less equal porous. The other types are unequally porous. Type B shows a wide range of pore radii with one maximum and is referred to as unimodal. In contrast, Type C is characterized by a second maximum of smaller pores and can be described as bimodal (Fig. 3c, f). The samples from Bentheim and Velpke represent Type A, whereas the Ibbenbüren, Heersum, Karlshafen, and Obernkirchen sandstones are of Type B. The remaining sandstones show bimodal distributions. The maxima in the pore size distribution of the analyzed samples correlate with their respective porosity. Sandstones with a high porosity exhibit a pore size frequency maximum in the range between 1.0 and 100.0 μm. Only the sandstone from Cotta, which is characterized by small detrital grains and a high amount of clay minerals, has its maximum between 0.1 and 1.0 μm. The other samples show with decreasing porosity also a decrease of pore size maximum (cf. Table 2). From the pore radii distribution, the average pore radius was also calculated. For this purpose, the pore radii classes were weighted according to their portion of the total porosity. The values vary between 0.04 μm for the Barkhausen sample and 9.59 μm for the Ostlutter sandstone. For the average pore radius

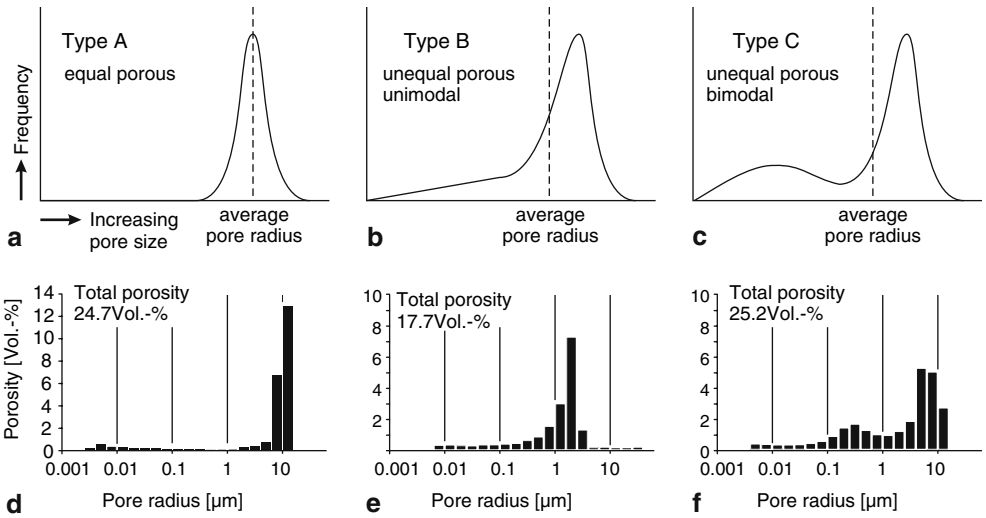

Fig. 3 Pore radii distribution: **a–c** idealized pore radii distribution types for sandstones and **d**, **e** respective pore radii distributions of the investigate samples (**d** Bentheim, **e** Obernkirchen, **f** Cotta)

also a good connection with the porosity of the respective rock exists (Fig. 4a).

In order to constrain the directional dependence of capillary water absorption, the same device as for buoyancy weighting was used, but the specimens were dipped only 0.5 cm into water. The measurements have been carried out on sample cubes ($65 \times 65 \times 65$ mm) cut according to the three principal directions (X, Y, Z) of the reference coordinate system. Thus, directionally dependent measurements can be performed on one sample. The water absorption coefficient (w-value) was calculated from the capillary water absorption data (Table 3). The w-value of the investigated sandstones varies between 42.6 and 0.3 kg/m$^2\sqrt{}$h. In Fig. 4b the water uptake coefficient is plotted against the average pore radius of the respective sample. It is obvious that

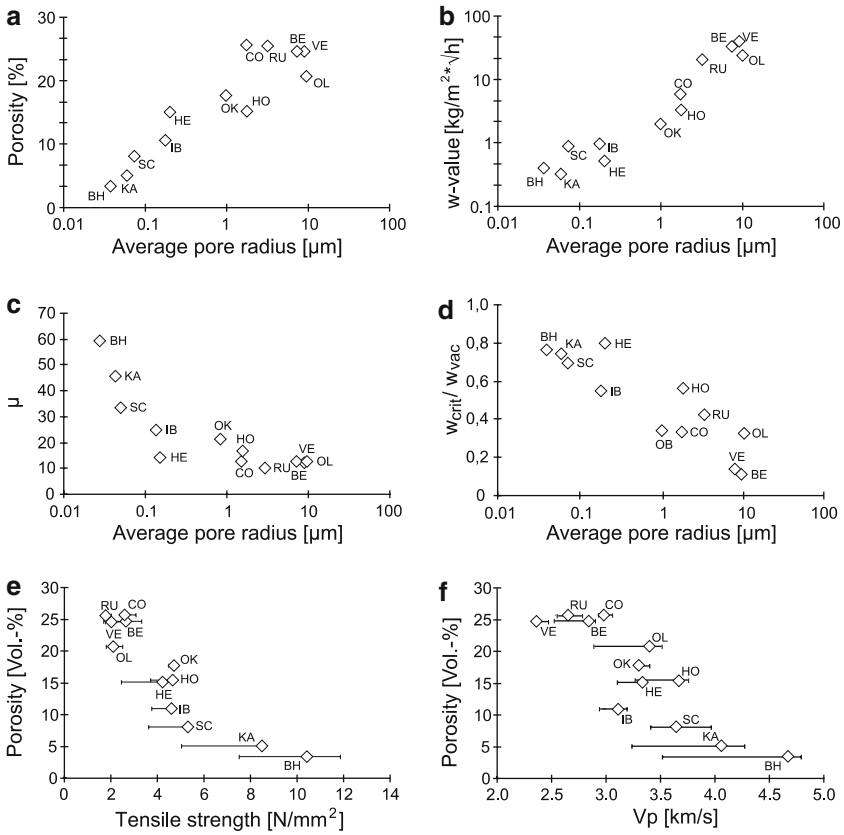

Fig. 4 Correlations of petrophysical properties of the investigated sandstones (the *bars* in **e**, **f**) represent maximum and minimum data of the different stone directions, rock name abbreviations see Table 1)

Table 3 Moisture transport and restore properties of the investigated sandstones

Sandstone type	*w*-value				*μ*-value				*S*-value	w_{crit}/w_{vac}
	X	*Y*	*Z*	*A* (%)	*X*	*Y*	*Z*	*A* (%)		
Cotta	6.9	6.1	4.9	29.0	12.72	12.08	13.36	9.6	0.65	0.3
Ruethen	20.4	22.4	18.2	18.8	10.39	9.84	10.16	5.3	0.79	0.3
Bentheim	40.7	42.6	36.9	13.4	11.64	11.62	13.01	10.7	0.72	0.1
Velpke	31.5	33.4	35.3	10.8	12.60	12.91	12.23	5.3	0.77	0.1
Ostlutter	24.9	21.7	28.3	23.3	11.17	9.30	18.14	48.7	0.80	0.3
Obernkirchen	2.1	2.0	1.9	9.5	21.52	21.31	21.04	2.2	0.61	0.3
Hockeln	3.3	3.4	2.5	26.5	13.92	16.26	20.20	31.1	0.69	0.6
Heersum	0.4	0.5	0.7	42.9	11.53	17.41	13.98	33.8	0.81	0.8
Ibbenbueren	0.9	1.0	0.8	20.0	26.04	22.55	26.76	15.7	0.77	0.6
Schoetmar	0.9	0.9	0.9	0.0	31.98	35.68	32.84	10.4	0.79	0.7
Karlshafen	0.3	0.4	0.3	25.0	45.83	40.48	49.81	18.7	0.63	0.7
Barkhausen	0.4	0.4	0.3	25.0	55.75	50.05	71.97	30.5	0.50	0.8

samples with a high average pore radius have a pronouncedly higher *w*-value compared with sandstones which exhibit a low average pore radius.

The water vapour diffusion resistance value (μ) of the sandstones was studied using the wet-cup method. μ characterizes the diffusion resistance of a porous material compared to an equally dimensioned inactive air film. Slices of the stones were attached as covers on teflon cups. The relative humidity on the outside and inside of the cups was different. This causes moisture to flow through the porous material from the side with higher (inside 100%) to the side with lower relative humidity (outside 50%). The moisture flow was obtained by weighing the cups at various times. Beside the capillary absorption the diffusion of water vapour is the second important water transport mechanism of porous materials. The non-dimensional water vapour diffusion resistance value (μ), which is normally used to describe the measure of water vapour diffusion, varies in the range between 10.2 and 72.0 for the investigated samples (Table 3). Also for this rock parameter, the correlation with the median pore radii diameter holds true, and thus, the pore radii distribution mainly controls the water vapour diffusion (Fig. 4c).

To get information of the critical moisture content (w_{crit}) of the investigated sandstones, we performed evaporation experiments. The critical moisture can be evaluated from the drying curve, which was measured by weighing against the time. The investigations were carried out with cubic samples ($65 \times 65 \times 65$ mm) which were vacuum water-saturated. The evaporation occurs by drying over all six cubic faces. The progressive loss of weight is linear in the first stage. At the point where the curve turns off and takes an asymptotical trend, the water content falls below the critical moisture. The ratio between point of critical moisture content and total saturation moisture (w_{crit}/w_{vac}) gives information about how fast the absorbed water can evaporate from the rock. Above the point of critical moisture content (w_{crit}), enough moisture can be capillary transported to the sample surface. Below this point the drying is controlled by the water vapour conductivity of the respective sandstone. For the investigated samples, the critical moisture content varies between 0.1 and 0.8 (Table 3). These pronounced differences are caused by the large range of pore space properties of the investigated sandstones. However, a dependency between the w_{crit}/w_{vac} value and the average pore radii is observable (Fig. 4d).

The tensile strength (σ_z) was determined by means of the ''Brazilian test'', which involves disc-shaped specimens. The samples were 40 mm in diameter and 20 mm in length. In order to calculate the average value, a minimum of four samples was used. A constant strain rate of 0.3×10^{-6} mm s^{-1} ($\approx 10^{-5}$ s^{-1}) was applied. The tensile strength was measured perpendicular to the *XY*-, *XZ*-, and *YZ*-plane. The resistance of sandstones against tensile stresses is an important parameter for salt and frost weathering, because the induced stresses by crystallisation have to exceed the tensile strength before damage occurs. The tensile strength varies for the different sandstones types between 1.82 and 11.57 N/mm^2 (Table 4). A correlation trend with the porosity is observable. Sandstones with low porosity show a high tensile strength and vice versa (Fig. 4e). Only the samples from Barkhausen and Karlshafen are characterized by a conspicuous anisotropy of the tensile strength.

Investigations of the compressional wave velocities (V_p) were performed to obtain information about the elastic properties of the sandstones. The transient times of ultrasonic pulses (piezoceramic transducers, resonant frequency 250 kHz) were measured using the transmission technique (Birch 1960, 1961). The measurements were carried out at cubic samples

Table 4 Tensile strength and ultrasonic velocities of the investigated sandstones

Sandstone type	Tensile strength				Ultrasonic velocities (V_p)			
	$\perp XY$ (N/mm^2)	$\perp XZ$ (N/mm^2)	$\perp YZ$ (N/mm^2)	A (%)	X (km/s)	Y (km/s)	Z (km/s)	A (%)
Cotta	2.68	3.16	2.71	15.3	3.0	3.0	2.9	3.3
Ruethen	1.82	2.16	1.93	15.5	2.7	2.8	2.6	6.7
Bentheim	1.84	3.40	2.76	45.8	2.9	2.9	2.6	10.3
Velpke	1.93	2.87	2.16	32.9	2.4	2.4	2.3	4.2
Ostlutter	1.96	2.62	2.23	25.2	3.5	3.4	2.8	20.0
Obernkirchen	4.51	5.09	4.74	11.5	3.3	3.4	3.2	5.9
Hockeln	3.77	4.70	4.67	19.9	3.7	3.7	3.4	8.1
Heersum	2.56	4.74	4.27	45.9	3.3	3.3	3.1	14.7
Ibbenbueren	3.82	4.63	4.75	19.5	3.1	3.2	2.9	5.9
Schoetmar	3.70	5.31	5.35	30.9	3.6	3.9	3.4	12.8
Karlshafen	5.03	8.45	8.35	40.5	4.0	4.2	3.2	23.8
Barkhausen	7.40	11.57	10.17	36.0	4.8	4.7	3.5	27.1

(65 × 65 × 65 mm). The compressional wave velocities of the investigated samples were mainly controlled by the rock fabric, because the mineralogical composition of the investigated rocks is more or less comparable (predominantly quartz). Based on this, the porosity should have the dominant influence, which is shown in Fig. 4f. For sandstones with a low porosity, V_p is about 2.3 km/s, whereas samples with a high porosity show ultrasonic velocities up to 4.7 km/s. The strong directional dependence of ultrasonic velocities for the Karlshafen and Barkhausen sandstones is remarkable (Table 4). For example, the Barkhausen sandstone shows compressional wave velocities of 4.7 km/s parallel and only 3.5 km/s perpendicular to the bedding, which represents an anisotropy (A) of 27.1% (calculated with $A = V_{pmax} - V_{pmin}/V_{pmax} \times 100$).

The hygric expansion of the sandstones was determined on cylindrical samples (∅ 15 mm × 50 mm), which were pre-conditioned at 30% relative humidity and room temperature. Afterwards, the samples were completely immersed in distilled water. The accuracy of the displacement transducer is 1.0 µm. The investigations were carried out on samples parallel to the X- and Z-direction. For the investigated samples, large differences of hygric expansion are observable (Table 5). Whereas the sandstones from Bentheim, Velpke, Ostlutter, and Hockeln show only slight hygric expansion below 0.2 mm/m, the other samples exhibit a larger swelling above 0.2 mm/m.

Salt weathering

Salt crystallisation and mechanisms of salt deterioration

It has been known for a long time that salt attacks lead to the deterioration of porous building stones (Darwin 1839). However, the processes and driving forces of salt-induced deterioration are still under discussion. For an overview see Duttlinger and Knöfel (1993), Charola (2000), and Doehne (2002). Two main research fields of salt weathering can be distinguished: One of them deals with the crystallisation mechanisms of salt, i.e. under what conditions and how exactly do salts develop from a solution. The other one focuses on the deterioration mechanisms of salt, which describe how salt crystallisation in porous materials might cause stress.

To the most part, the salt crystallisation mechanisms are influenced by the properties of the salt solution, the properties of the growing salts, the climatic conditions, and the properties of the substrate. The cause for salt formation in porous rocks is the existing of unbounded elements. This loading takes place due to chemical alteration of existing solid phases or due to external supply. The solid phases are the rock itself or surrounding materials like mortars or conservation materials formerly used. The main ionic entries are

Table 5 Hygric dilatation of the investigated sandstones

Sandstone type	Hygric dilatation			
	X (mm/m)	Y (mm/m)	Z (mm/m)	A (%)
Cotta	0.07	0.08	0.13	46.1
Ruethen	0.15	0.22	0.41	63.4
Bentheim	ND	ND	0.02	ND
Velpke	0.06	0.07	0.08	25.0
Ostlutter	0.02	ND	0.02	ND
Obernkirchen	0.06	0.08	0.13	53.8
Hockeln	0.11	0.08	0.11	23.1
Heersum	0.32	0.35	0.48	45.7
Ibbenbueren	0.31	0.30	0.35	14.3
Schoetmar	0.79	0.84	1.13	30.1
Karlshafen	0.50	0.62	1.04	51.9
Barkhausen	0.57	0.46	0.83	44.6

ND not detectable

usually activated by the external loading, mainly through capillary water transportation but also through air pollution (corrosive gases like SO_x and NO_x as well as dusts and sooty particles). The ionic origin can have either natural sources, e.g. soils, or anthropogenic features such as fertilizer and de-icing salt. Concerning the salt weathering, the cations Na^+, K^+, Mg^{2+}, Ca^{2+} und NH^{4+} as well as the anions CO_3^{2-}, Cl^-, SO_4^{2-} und NO^{3-} are of crucial importance since they are the constituents of most masonry salts (Arnold and Zehnder 1990). The ionic transportation in the rock's pore space takes place predominantly in aqueous solutions. The respective consistency of the solution controls its physical properties, like viscosity, surface energy, and vapour pressure, which have crucial influence on the dynamics of the migrating solution and the evaporation inside of the stone (Pühringer and Engstrom 1985).

The ionic supply of the aqueous solution and the thermodynamic properties like temperature and water vapour partial pressure are responsible for the crystallisation of a specific salt type. Crystallisation takes place if the solution is super-saturated, i.e. the solubility of the respective salt is exceeded. Super-saturation can be reached either by evaporation or temperature changes (for salt types with a thermal dependency of their solubility; Rodriguez-Navarro et al. 1999). In most cases, it is salt mixtures that appear on the building. This leads to ionic interactions, and thus, the crystallisation properties and solubility can strongly differ from pure salt solutions (Steiger et al. 1998). The varying solubility of each salt type leads to a fractionation of salt solution on buildings. The result is a typical distribution of salt phases found in masonry (see Arnold and Zehnder 1990).

About 50 salt types commonly appear on buildings. Characteristically, the salt types have very different physical and chemical properties. Of particular importance is the formation of the hydrate phases of several salts. Sodium sulphate is a known example for appearing as thenardite (Na_2SO_4) when water-free and being able to change to the water-rich salt phase mirabilite ($Na_2SO_4{\cdot}10H_2O$). A further important property is the hygroscopic behaviour of salts. This means the absorption of water vapour from the air, which can be traced back to vapour pressure decreasing above a salt solution. A degree of the hygroscopic behaviour is the deliquescence moisture, which occurs above a saturated salt solution. By exceeding the deliquescence humidity, which causes a pronounced mobility of salts under certain environmental conditions, the hygroscopic properties of salts can lead to the dissolution of salts.

In addition to that, the climatic conditions have a crucial influence on the salt crystallisation. The temperature, the relative humidity, and the air flow determine the evaporation rate, and therefore, the super-saturation of the salt solution as well as the nucleation and growing rate. Furthermore, the stone's properties are important to the manner of salt weathering (see Fitzner 1969).

The pore space's properties, such as the porosity, pore radii distribution, pore shapes, and pore interaction control the solution transportation and restore the behaviour of the rocks. In consequence, these material characteristics are responsible for the salt's distribution and enrichment in the rock (cf. Snethlage and Wendler 1997). Fitzner and Snethlage (1982) found out that the pore size distribution is of crucial importance. Their investigations on various German sandstones show that samples with a large amount of smaller capillary pores and micro-pores (e.g. bimodal pore size distribution) are extremely susceptible to salt attack (see also Zehnder and Arnold 1989; Rossi-Manaresi and Tucci 1991). Salt resistibility tests done by Ruedrich et al. (2005) also demonstrated that rocks with a relatively low tensile strength are less resistant.

Investigations by Zehnder and Arnold (1989) on the dynamics of crystal growth inside a pore (considering the crystallographic properties of the salt type) show that the shape of the crystal and its growth rate has an important influence on the pattern and intensity of the damage to the rock. Sunagawa (1981) found that the shape and morphology of a growing crystal depends on the supersaturation rate. According to Rodriguez-Navarro and Doehne (1999) the factors discussed above should control the salt crystallisation, i.e. the location and distribution depends on the respective salt type. They demonstrated that, under the same experimental conditions, halite might show efflorescence, whereas thenardite crystallise within the pore space.

The salt deterioration mechanisms describe how stresses may be created due to salt crystallisation in porous materials. There are different models suggested in research literature to explain stress development. As introduced by Correns and Steinborn (1939) and Correns (1949), the linear crystal growth pressure will develop if a crystal grows against the surrounding pressure and if there is a thin, super-saturated solution film between the pore surface and the salt crystal (Taber 1916). The increasing growth pressure is mainly controlled by the super-saturation of the surrounding solution. Crystallisation pressures of different salts have often been calculated by applying the equation by Correns and Steinborn, as frequently cited in literature (Winkler 1975), although they require extremely high

super-saturation ratios between 2 and 50. Snethlage (1984) has already suggested that these super-saturation ratios are extraordinarily high due to the multiple possibilities of heterogeneous nucleation within natural rocks. However, calculations by Steiger (2005) show that a 1.05 supersaturated NaCl solution is sufficient to generate pressure of 15 MPa, i.e. exceeding the tensile strength of all stones presented in this manuscript. Wellmann and Wilson (1965, 1968) provide another approach, which is based on a thermodynamic model. They assumed that crystal growth takes place in larger pores first, which was confirmed by Putnis and Mauthe (2001). More recently, Steiger (2005) has also presented an updated discussion on the origin and nature of crystal growth pressure. The properties of the growing crystals could be of crucial importance (cf. Scherer 1999) to the stress development within the pore space.

Mortensen (1933) was the first one to introduce the kind of hydration pressure that develops if the volume increases upon the hydration of salt. Based on the proposed model by Mortensen et al. (1970) calculated the resulting hydration pressures of different salt types. These high pressures may only be true if they are of osmotic nature (see Discussion in Duttlinger and Knöfel 1993). They suggest a modified model, based on the literature mentioned by Mortensen, which results in lower hydration pressures. The damage potential could also be controlled by the hydration/dehydration reaction, especially in the complex pore spaces of natural rocks (Duttlinger and Knöfel 1993). For example, some findings prove that the dehydration of mirabilite to thenardite takes place at multiple stages of dissolution (Charola and Weber 1992; Doehne 1994). On the other hand, the hydration of thenardite will slow down if there is a thin hydrated film on the salt surface. However, for salts with a hydration phase, it is still questionable which process (crystallisation or hydration) may cause the higher damage potential (Chatterji et al. 1979; Sperling and Cooke 1980).

There are also other hypotheses on how salt can account for the damage to natural rocks, e.g. differences in the thermal dilatation between the salt and the rock minerals (Winkler 1994). The thermal expansion coefficient of halite is four times larger than the one of quartz (cf. Skinner 1966). If there is a large amount of halite in the pores, temperature changes can also produce stresses on the rocks. In contrast to that, Pühringer (1983) suggested that the crystallisation and recrystallisation of thin salt layers might result in shearing stress, which would lead to an ''erosion'' of the substrate. Snethlage and Wendler (1997) suggest that it is the hygric expansion in combination with salt loading that mainly determines the decay of clay-containing sandstones. Due to the swelling of the clay minerals, the pore spaces grow and salts could spread. The fabric cannot return to its initial position during drying, which results in a residual strain. Even hydraulic pressure generated as a result of volume expansion and often quoted as a relevant damage mechanism for frost damage has been discussed also in the context of salt damage by various authors (e.g. McMahon et al. 1992).

Laboratory results of salt weathering

Salt crystallisation test

In order to provide information about the fabric dependence of salt weathering, salt crystallisation tests according to the German VDI 3797 standard were performed. The investigations were carried out on cubic samples (65 mm edges length), which were cycle-loaded with a sodium sulphate (10%) solution. For the capillary solution uptake, a period of 4 h was chosen, and the drying required 16 h at 60°C in a drying chamber. After a cooling phase of 2 h, the loaded samples were weighed. For the investigations, two samples of each sandstone type were used.

Sodium sulphate is a frequent masonry salt and can be considered as extremely destructive (Doehne 1994; Rodriguez-Navarro et al. 2000). From the sodium sulphate solution, two crystal phases can develop. The water free-phase, thenardite (Na_2SO_4), and the hydrate phase, mirabilite ($Na_2SO_4 \cdot 10H_2O$). The phase transition from thenardite to mirabilite at water absorption is associated with a volume increase of about 300% (Price and Brimblecombe 1994). This hydration process takes place in a climate range which is often found in nature (Steiger et al. 1998). The conversion at 20°C takes place at 75% relative humidity, whereas thenardite is stable in the lower and mirabilite in the higher humidity range (Fig. 5). The hydration process normally takes place during a short period.

The main criteria of weathering resistance in the tests are the visible changes of the sample surfaces, the change of weight after each cycle of loading, and the change of ultrasonic velocities. To get further information about the change of pore space after the salt crystallisation test for the respective sample, investigations using a scanning electron microscope (SEM) were carried out. For the various sandstone samples, differences of salt distribution (efflorescence or subflorescence), damage forms, and material loss behaviour are observable during the salt crystallisation

tests. These differences can be attributed to the respective fabric properties and petrophysical parameters. It seems that the porosity and the pore size distribution have the main influence on the resistance of the sandstones in the salt loading test.

After drying, the sandstone types show different efflorescence. Whereas the samples with a high porosity from Cotta, Ruethen, Bentheim, Velpke, and Ostlutter reveal a lot of salt at the cubic surface, the other samples exhibit only moderate or slight efflorescence. Besides the amount of salt which crystallises at the surface, also the location of efflorescence on the sample surface differs. For sandstones a with medium to low porosity from Heersum, Ibbenbueren, Schoetmar, Karlshafen, and Barkhausen, efflorescence was localized at the edges of the cubic specimen. For the other samples, a preferred salt crystallisation at the faces are observable. Thus, the different rock properties control the amount and location of efflorescence and, therefore, also the enrichment of salts within the samples.

Besides the differences in salt distribution, also varying damage phenomena are observable. For most samples, the damage in form of sanding lead to a rounding of the cubic edges and an increasing backweathering of the surfaces, whereas the intensity of deterioration varies. In contrast to sanding, the sandstones from Schoetmar, Heersum, and Karlshafen showed scaling after a certain number of loading cycles. The thickness of the scales is between 5 and 10 mm. For the Barkhausen sandstone, a cracking along the bedding occurred after 41 loading cycles, which leads to a disc-like deterioration. The different damage phenomena correspond with a special pattern of material loss. Whereas samples which are characterized by sanding show a more or less linear decrease in weight, samples which exhibit scaling or cracking show a constant weight over several loading cycles followed by a spontaneous decrease in weight caused by the loss of scales or discs. This is shown exemplarily for the sandstones from Velpke and Schoetmar in Fig. 6. The observable increase in weight in the first load cycles is caused by salt enrichment within the pore space of the porous material without sample deterioration.

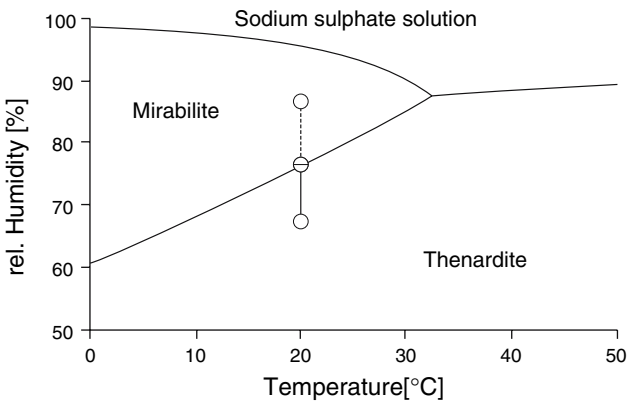

Fig. 5 Temperature and relative humidity stability ranges of sodium sulphate (from Steiger and Dannecker 1998)

The different damage phenomena can be traced back to pore space properties of the investigated samples. Sandstones which are characterized by a relatively slow drying rate show scaling as main damage phenomenon. In contrast, sandstones with a high drying velocity exhibit sanding. A corresponding petrophysical parameter is the critical water content (w_{crit}/w_{vac} value). For the presented salt crystallisation tests, samples with a w_{crit}/w_{vac} value over 0.6 show scaling (Schoetmar, Heersum, Karlshafen, and Barkhausen) and below 0.6 sanding as main deterioration phenomenon (Table 3).

Since for all samples the experimental conditions are similar in the crystallisation tests, differences in the mineralogical composition or the fabric properties should be responsible for the varying resistance within the test. In order to correlate the petrophysical properties of the sandstones with their weathering resistance in the salt crystallisation tests, the cycle in which the samples achieve a decrease in weight of 10% of their initial weight were used (highest value of two investigated samples). In Fig. 7 the respective loading cycles of samples are plotted against their tensile strength and their accessible porosity in the non-weathered condition. In general, it can be concluded that sandstones with a high porosity stay only few cycles within the crystallisation test. Thus, samples with a high porosity should be more sensitive to salt growth in the pore space in contrast to sandstones with a low porosity. However, there are exceptions, which can be traced back to the different pore size distributions. The respective pore radii types, which correlate with the different sandstones, are marked with symbols in Fig. 7. It can be determined that samples with the pore space distribution of Type A stay more cycles, corresponding to their porosity and their tensile strength, than the samples of pore radii Type B and C. This points out that samples with a distinct pore radii maximum besides a low amount of micro pores are more resistant against salt loading.

Analyses of the ultrasonic velocities are a helpful tool to characterize material changes. As discussed above, V_p strongly depends on the porosity of the sandstones. Thus, the filling of pore space should lead to an increase of ultrasonic velocities. In contrast, a

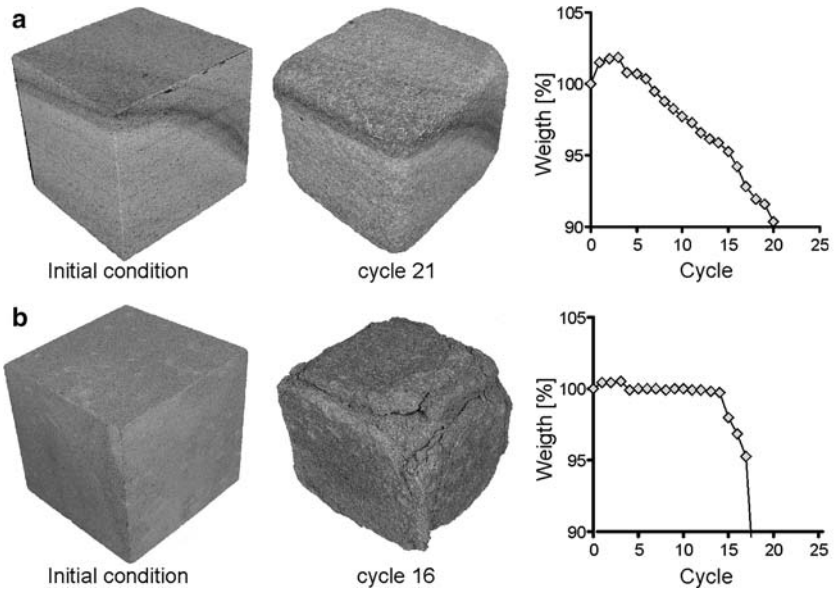

Fig. 6 Damage phenomena and damage progress during salt crystallisation test: initial and weathering state after a certain number of loading cycles and the respective loss in weight for the **a** Ibbenbueren and **b** Schoetmar sandstone. Remarkable are the different weathering phenomena (sanding of the Ibbenbueren and scaling of the Schoetmar sandstone), which caused the different weight losses

fabric deterioration caused by salt attack should result in a decrease of V_p.

For the investigated sandstones, two different behaviours of V_p during the salt crystallisation tests are observable. The samples from Bentheim, Velpke, Obernkirchen, and Barkhausen reveal a pronounced increase of V_p up to the third loading cycle, which is exemplarily shown for the Bentheim sandstone in Fig. 8a, b. In the subsequent cycles, the velocities decrease slightly. The changes of sample weight show similar behaviour compared with the ultrasonic velocities. Thus, for these sandstones a salt enrichment occurs in the initial state, which does not lead to measurable deterioration. The other sandstones show a more or less strong decrease of V_p up to the third test cycle, whereas in subsequent cycles the decrease is only slight. However, the changes in weight of the samples differ from the development of ultrasonic velocities. Although V_p decreases up to the third test cycle, the weight of the samples increases. As an example for this behaviour, the Cotta sample is shown in Fig. 8c, d. Therefore, the sandstones which reveal this behaviour exhibit fabric deterioration from the beginning of the test. Moreover, the decay affects V_p more than the enrichment of salt within the pore space of the sandstones.

For the Barkhausen sandstone, a strong anisotropic behaviour of the ultrasonic velocities is observable (Fig. 8e, f). Parallel to the bedding, no significant changes of V_p with about 4.8 km/s are observable. In contrast, perpendicular to the bedding, a strong increase of velocities from 2.0 to 4.0 km/s occurs up to the ninth cycle. This phenomenon can be traced back to a preferred orientation of pore space, which was filled by salt without a significant deterioration. Subsequent to the ninth test cycle, the velocities decrease and reveal the beginning of deterioration induced by salt loading. Remarkable is that the first visual damage occurs in cycle 38. Thus, the sensitivity of V_p is sufficient to detect the beginning of fabric deterioration before a macroscopically decay is observable.

The occurrence, distribution, and morphology of salt crystals within the pore space after the crystallisation

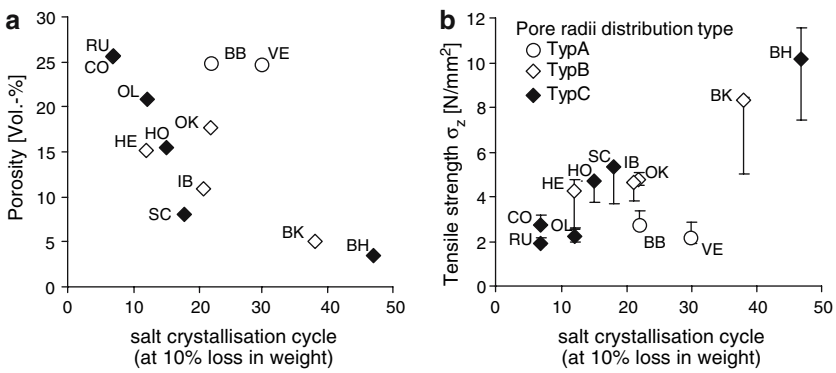

Fig. 7 Relative resistance of sandstones from the salt crystallisation test and the dependence on rock physical properties: number of loading cycles for 10% weight loss for the respective sample versus **a** porosity and **b** tensile strength (the *bars* represent maximum and minimum data of the different stone directions)

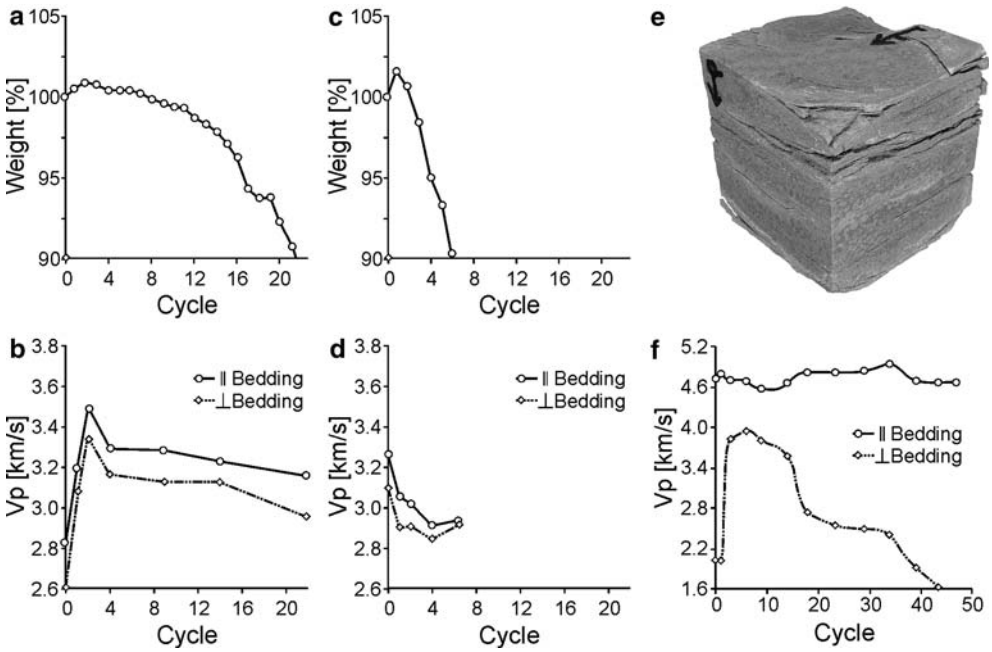

Fig. 8 Changes of ultrasonic velocities (V_p) induced by the salt crystallisation test: weight changes (**a**, **c**) and changes of the ultrasonic velocities (**b**, **d**) during cyclic salt loading for cubic sandstone samples from **a**, **b** Bentheim and **c**, **d** Cotta, **e** disk-like deterioration along the bedding of a Barkhausen cube after 48 salt loading cycles and **f** the respective ultrasonic velocities

tests were analyzed by SEM investigations (fractography). For samples which went through only few loading cycles, isolated crystals, which occur in local accumulations, are observable. This is exemplarily shown in Fig. 9a for the Cotta sandstone after seven salt loading cycles. The shape of the crystals is euhedral to subeuhedral. The frequent occurrence of isolated crystals reveals a heterogeneous nucleation. This indicates only low supersaturating of the salt solution at the beginning of crystallisation (Snethlage 1984). For samples which went through numerous loading cycles, salt is strongly enriched within the rock. The sodium sulphate in the pore space of the Bentheim sample covers the pore walls and seems like a ''crystal lawn'' (Fig. 9b). This Bentheim specimen went through 24 salt loading cycles. The salt crystals show sub-euhedral morphologies that suggest 3D growth mechanisms (Sunagawa 1981). Only in some areas did the sodium sulphate crystals have the appearance of a thin salt film which lies on the surface like a ''cloth'' (Fig. 9b). Since the sampling of the SEM specimens was carried out after 2 months of sample drying at 50% relative humidity, it can be expected that the occurring salt crystals consists of thenardite.

A major problem of the salt crystallisation tests described above is that two mechanisms are responsible for the change in weight of the samples. On the one hand, the cyclic loading leads to an enrichment of salt and thus to an increase in weight. On the other hand, the deterioration results in a loss of material and thus in a decrease in weight. Both mechanisms interfere with each other, and thus, no quantification of salt enrichment or of the loss of material during the test can be made if only the whole sample weight is measured. Based on this, a second modified crystallisation test was performed. During salt solution uptake and also during drying of the samples, the detached material was collected separately for each sample. The material gathered was then desalted by rinsing it out with demineralised water. This approach allows the detection of the real loss of material of every specific sample as well as the calculation of the salt enrichment by subtraction from the initial mass of the sample.

The results of this test are shown in Fig. 10 for the Velpke, Bentheim, Ruethen, and Cotta sandstones, which were loaded over seven cycles. The selected sandstones have more or less a comparable porosity but differ in their pore radii distribution (Table 2). The development of the whole sample mass during cyclic loading is comparable with the standard test (Fig. 10a). The Velpke and Bentheim sandstones show only a decrease of mass during the seven cycles. The other sandstones from Ruethen and Cotta only exhibit a mass increase in the first cycle followed by a decrease of mass in the further cycles. The calculated real mass of the sandstone samples without the salt content reveals in the first three loading cycles more or less no mass changes (Fig. 10b). In the subsequent cycles, a decrease of the sample mass is observable, which is strong for the Cotta and Ruethen sandstones and slight for the Bentheim and Velpke sandstones. The calculated salt enrichment shows that a large increase in weight results for all samples in the first loading cycle (Fig. 10c). The highest salt enrichment is observable

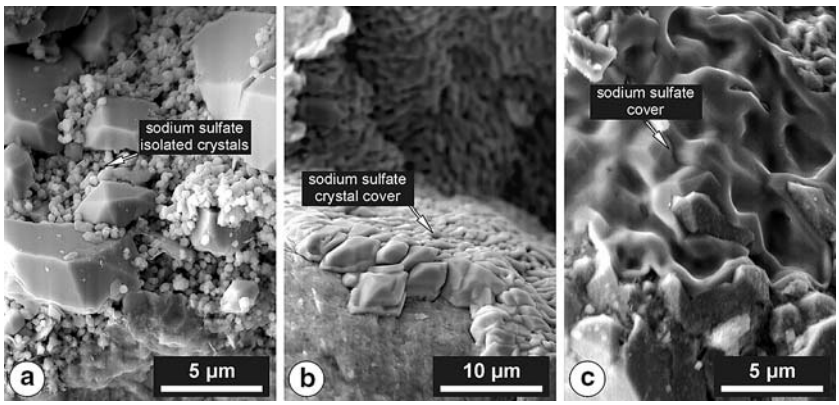

Fig. 9 Scanning electron microscope images of salt crystals within the pore space after the salt crystallisation test (fractography): **a** isolated small crystals after seven loading cycles in the Cotta sandstone and **b**, **c** different shapes of sodium sulphate covers at pore walls of the Bentheim sample after 22 loading cycles

for the sandstones from Bentheim and Velpke, whereas the Ruethen and Cotta sandstones exhibit low enrichment of salt. Remarkable is that the sandstones which are characterized by a high salt enrichment are only slightly affected by salt deterioration.

Length changes induced by salt crystallisation

In order to obtain detailed information about the weathering mechanisms and the stress development by salt crystallisation, simultaneous length change measurements during salt loading cycles were performed. The measurements were carried out with a dilatometer (Fig. 11), which allows independent control of temperature, humidity, and solution supply. The temperature and relative humidity were controlled by a climatic chamber through convective air circulation. Moreover, six samples can be analyzed simultaneously in one experiment. The length change behaviour of the sandstones was determined on cylindrical samples (∅ 15 mm × 50 mm) in two fabric directions: parallel (*X*-direction) and perpendicular (*Z*-direction) to the bedding. The accuracy of the incremental displacement transducers used is 1.0 µm. The studies were carried out with a 10% sodium sulphate solution. The solution absorption was obtained over a 4-h period using a capillary uptake through several layers of cellulose. Following this, the samples were dried for over 16 h. The evaporation of the water and therefore the supersaturation and crystallisation were achieved by a constant low relative humidity of 30% at 20°C ambient temperature. This approach was chosen to avoid the influence of temperature on the length change, another possible deterioration mechanism. The length change behaviour is exemplarily described in the following for the sandstones from Schoetmar, Cotta, and Ruethen.

During the absorption stage in the first five loading cycles, the Schoetmar sandstone shows an obvious hygric expansion in the presence of the sodium sulphate solution (Fig. 12a; cf. Table 3). After drying, a residual strain remains, which is probably caused by the incorporation of sodium ions in the interlayers of clay minerals. Starting with the ninth cycle, the dilatation shows a strong increase during solution uptake. Also, a strong increase of the residual strain is observable, which results in a large material loss. After the thirteenth cycle, the cylindrical samples of this sandstone are more or less completely deteriorated.

The length change of the sandstone from Cotta is characterized by a different behaviour in the two sample directions during sodium sulphate solution loading (Fig. 12b). Up to the eighth cycle, the sample which is oriented perpendicular to the bedding plane shows a slight expansion during the solution uptake and a contraction in the drying stage. This results in a continuous slight contraction of the specimens. After the eighth cycle, a larger expansion is observable, which results in an obvious residual strain. After the

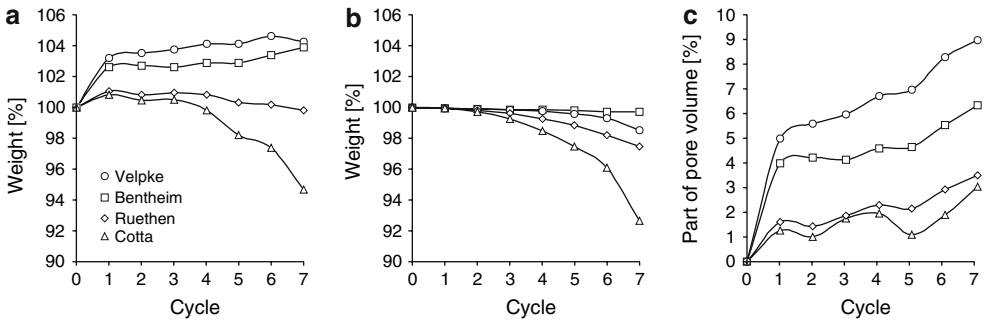

Fig. 10 Change in weight and salt enrichment from the modified salt crystallisation test, exemplarily shown for the Bentheim, Velpke, Ruethen, and Cotta sandstone: change in weight for **a** the whole samples (salt inclusive), **b** the sandstone without salt, and **c** salt enrichment in the different samples

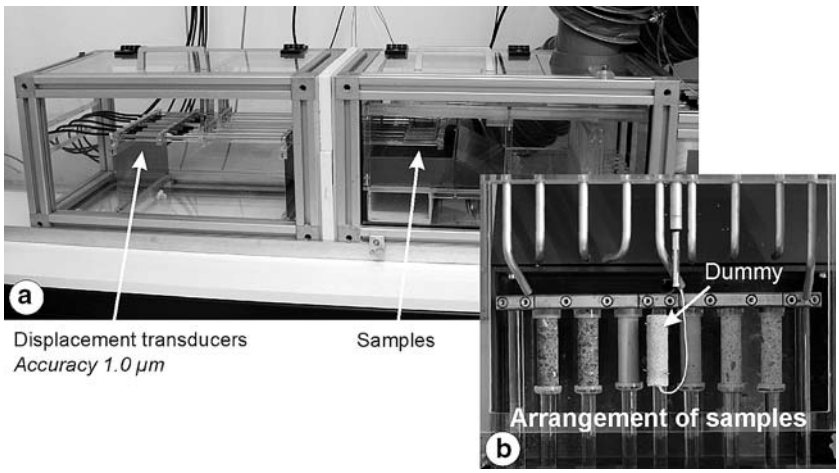

Fig. 11 Dilatometer with climatic control for the length change measurements of porous solids during salt and frost loading

twelfth cycle, this sample was deteriorated. The sample parallel to the bedding is characterized by a very slight expansion during the absorption stage and a slightly stronger contraction after drying. This behaviour leads to a continuous shortening of the samples.

In contrast to the samples described above, the Ruethen sandstone reveals increasing contraction during the test in both sample directions (Fig. 12c). The increasing shortening of the samples result from a slighter expansion in the wetting stages and a generally larger contraction in the drying stages. This behaviour is observed for both sample directions during the first 13 loading cycles. Remarkably, a total contraction up to 1 mm/m was determined. At this time, the cause of the pronounced material shortening remains unknown.

The length change measurements allow the assumption that hydration of Thenardite to Mirabilite is the main cause of damage. In Fig. 13, the first and the thirteenth cycle of the Schoetmar sandstone in both fabric directions is shown. The expansion in the first drying stage is clearly connected with hygric swelling of the clay minerals. In contrast, the expansion by solution uptake in the thirteenth cycle is more than three times higher. This can be attributed to hydration of the water-free salt phase. However, at the beginning of the drying state, further expansion appears, and thus, stress development by crystallisation mechanisms could also be subordinately involved in the damage process.

Frost weathering

Ice crystallisation and ice deterioration mechanisms

Frost weathering, in addition to salt weathering and thermal and hygric dilatation, is a major physical deterioration process of historic masonry. Alternating freeze and thaw cycles are held to be responsible for most damage during winter. Numerous freeze and thaw cycles can occur in Central Europe (e.g. in Germany sometimes over 30 per year). A further precondition for this damage mechanism is the availability of water in the pore space. This can occur during specific weather phenomena, e.g. intense rainfall and subsequent cooling below the freezing point.

The mechanisms of ice crystallisation and growth have been the subject of research for several decades. Super cooling is responsible for the crystallisation from a melt (water, in this case). It can be assumed that a main mechanism of stress concentration in the rock fabric is the volume expansion induced by the phase transition from water to ice (9 Vol% under atmospheric conditions). Based on this fact, a porous rock with more than 91% water content could sustain direct frost damage (Hirschwald 1908). Thus, rocks with a saturation degree of voluntary water absorption of more than 90% should be extremely vulnerable to frost action. The maximum pressure achieved for a super cooling of around –22°C is about 200 N/mm^2 (Winkler 1968). This value is much higher than the tensile strength of natural building stones. The significance of damage development by pure volume expansion is still under discussion because most rocks in nature do not reach such high water saturation and, further, many rocks with a saturation of less than 90% are affected by frost action. Due to this insufficient explanation for the stress development during ice crystallisation in the pore space of rocks, two other models will be discussed. These are the models of linear growth pressure (Scherer 1999) and the capillary pressure model (Everett 1961).

Numerous natural observations of ice crystallisation that support the model of linear growth pressure as a main damage mechanism exist (cf. Scherer 1999; Stei-

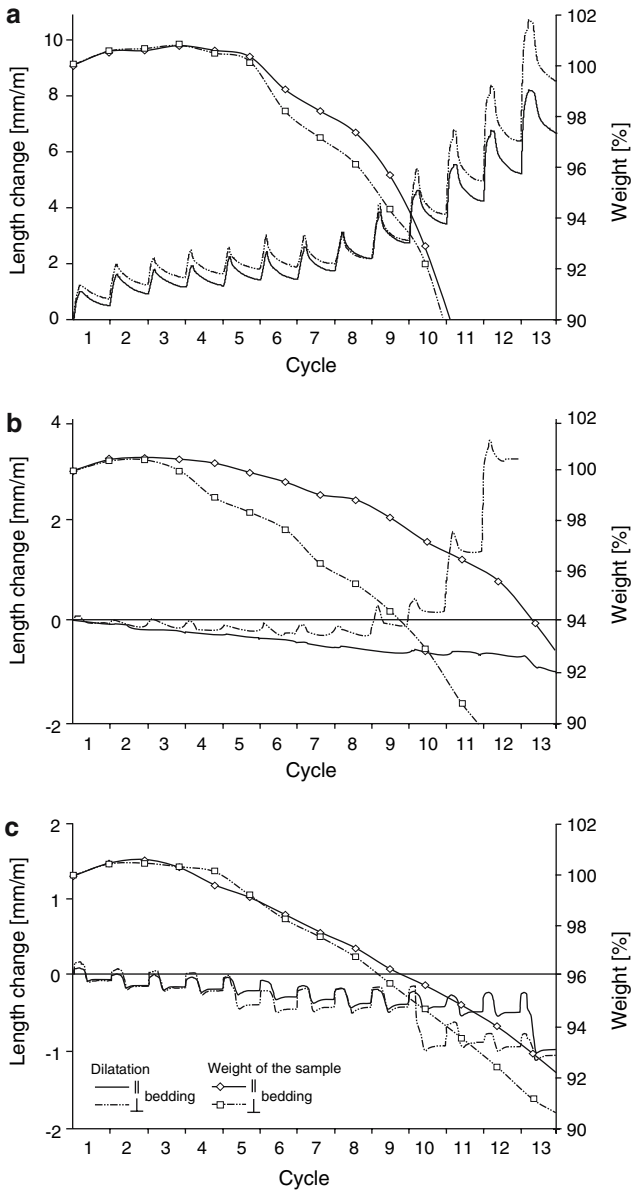

Fig. 12 Length change behaviour of sandstone samples parallel and perpendicular to the bedding during salt tests with sodium sulphate for thirteen loading cycles and the respective loss in weight for **a** Schoetmar, **b** Cotta, and **c** Ruethen sandstone (for explanations see text)

ger 2005). For example, growing ice crystals can transport other solids onward in front of it. It was proven that for this purpose, a thin film of water between the growing ice and the other solid is necessary. The driving force for this process is the rate of super cooling (cp. Winkler 1994).

The capillary pressure model is based on the knowledge that crystallisation first takes place in larger pores since water in smaller pores allows a larger super cooling before ice crystallisation starts (Everett 1961). In the case of a supply of water from smaller pores, but also from rock areas that are not affected by freezing, water could be available for ice crystallisation in larger pores. However, Everett's frost model is identical with the Wellmann and Wilson approach for salt damage. Moreover, it was shown recently by Steiger (2005) that supersaturation is also the driving force in Everett's model.

Further theories about the stress development by ice crystallisation in porous material exist. Powers (1945, 1949) introduce that hydraulic pressure could be the cause for stresses in the fabric. This consideration based on the observation that ice crystallises as moving front into the rock. Due to the volume increase of ice, unfrozen water can be pressed in the pore space. If not enough expansion space close to the ice front is available, stresses were generated in the fabric. Further models for stress development are based on osmotic pressures (Powers 1955) and an anomalous density behaviour of ice during fast crystallisation (Kiseleva et al. 1975).

Advanced considerations assumed that different processes could occur simultaneously or chronological shifted, depending on the pore space properties of the rock and the moisture distribution (Stockhausen 1981). For example, during fast cooling, the crystallisation in a larger pore can seal a micro-pore so that a connection to other pores no longer exists. Further, fast cooling and an extensive filling of micro pores results in high pressure only with pure volume expansion of growing ice. In contrast, with slow cooling a sealing of smaller pores in combination with a diffusion of water to the crystals in larger pores could result in a negative pressure and thus in a shortening of the porous material (Weiss 1992).

Results from laboratory tests

Freeze/thaw-test

In order to check the investigated sandstones' sensitivity to frost action, the samples were subjected to freeze/thaw cycles in the laboratory. For the loading, the used cubic samples ($65 \times 65 \times 65$ mm) were completely immersed in water (20°C) over a 4-h period. Following this, the samples were stored in a fridge at –20°C for over 16 h. To characterise the damage effect of the tests, measurements of ultrasonic velocities (V_p) were performed. Before analyzing the ultrasonic properties, the samples were dried in a drying chamber at 60°C until weight constancy was reached. The measurements were performed after every fifth cycle.

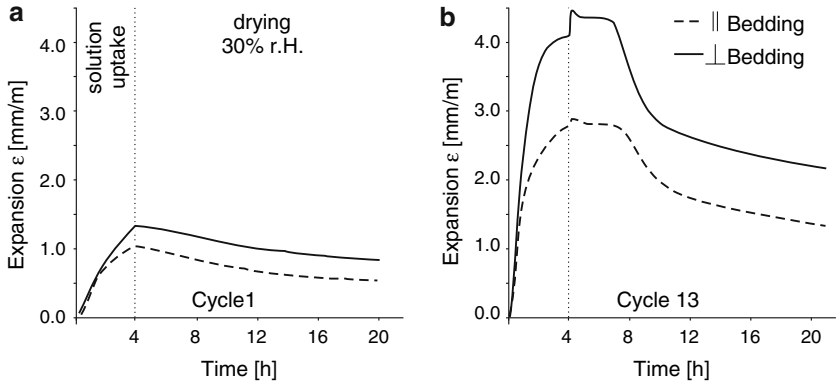

Fig. 13 Length change behaviour of the Schoetmar sandstone during salt tests with sodium sulphate in the first and thirteenth loading cycle (for explanations see text)

The results of the investigated samples show only slight changes of ultrasonic wave velocities. This is shown in Fig. 14a for some selected sandstone samples for 103 loading cycles. Only for the sandstone from Velpke do the ultrasonic velocities perpendicular to the bedding show a slight decrease after 80 freeze/thaw cycles. No significant change of V_p is observable for the other samples investigated. The sandstone from Hockeln, which shows a breakdown along a pre-existing partly mineralized crack after the fourteenth loading cycle (Fig. 14b), is an exception. This confirms that freeze/thaw tests preferred activate rock discontinuities, as is mentioned by some authors (e.g. Nicholson and Nicholson 2000).

Length changes induced by ice crystallisation

To provide detailed information about the weathering mechanisms of ice crystallisation within the pore space, simultaneous length change measurements during frost loading were applied. The measurements were carried out with the same dilatometer as used for the salt experiments (Fig. 11). The experimental setup allowed simultaneous investigation of six samples under comparable conditions. The length change behaviour was determined on cylindrical specimens (∅ 15 mm × 50 mm) in two fabric directions: parallel (*X*-direction) and perpendicular (*Z*-direction) to the bedding. To avoid moisture changes within the samples, the specimens were sealed with foil during the experiments (not shown in Fig. 11). A reference sample (dummy) was used to detect the sample temperature (Fig. 11). A temperature sensor was placed in a bore hole of the dummy for that purpose. Since the thermal conductivity is controlled by the mineralogical composition, the porosity, and the water content, the dummy was prepared from a comparable stone and was analogously conditioned. The temperature was also measured with a sensor above the samples within the chamber.

Samples in two different conditions were measured for the experiments: dry and water-saturated. Solution absorption of the samples takes place through capillary uptake. The vacuum method was used to fill the pore space with water in order to investigate the dependence on the degree of saturation. The samples were subsequently dried to the respective degree of saturation. The specimens were cooled from 20°C up to –20°C and back to the initial temperature. The temperature steps were held for 6 h each, respectively. The frost action test was normally carried out with a cooling rate of 0.5°C/min. In order to determine the dependence of length change behaviour on the degree of cooling, a cooling rate of 0.05°C/min was also compared.

The length change behaviour by cooling of water-saturated samples differs strongly compared to that of the dry samples. Under dry conditions, the samples show a more or less linear length change when cooling to –20°C as well as during subsequent heating up to 20°C. This behaviour is exemplarily shown for two sandstones in Fig. 15a, d. After returning to the initial temperature, no residual strain remains.

Two generally different length change types are observable (Type A and B) for water-saturated samples. They differ in the intensity and the shape of the curve. Both types are characterized by an expansion below the freezing point and a subsequent contraction. This contraction is stronger in the case of Type B and results in a great shortening of the sample compared to the dry sample behaviour. This is shown in Fig. 15b, e for the Velpke (Type A) and Ruethen (Type B) sandstones. The difference between dry and water-saturated samples is further plotted as length change difference diagrams (Δ length change) in Fig. 15c, f.

The dry and saturated samples of the Velpke sandstone do not show significant differences above the freezing point during cooling (Fig. 15a, b). Below the freezing point, at –2°C, a pronounced expansion occurs for the water-saturated samples and results in a peak

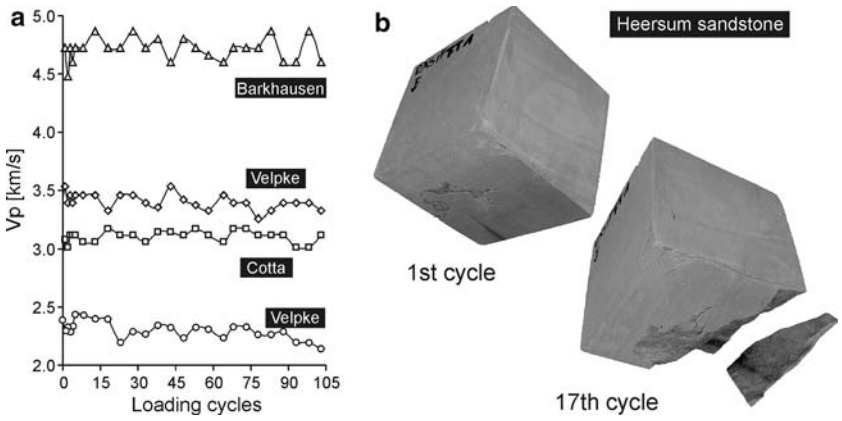

Fig. 14 Results of the freeze/thaw-tests: **a** change of ultrasonic velocities (V_p) for the Velpke, Cotta, Hockeln, and Barkhausen sandstone over 103 loading cycles and **b** breakdown of a Heersum sample along a flaw after 14 loading cycles

maximum at –10°C. The subsequent contraction is divided into two steps, whereas the first is stronger and reaches up to –13°C and the second is less pronounced. Both contraction steps are stronger than the contraction observed under dry sample conditions.

In the subsequent heating, the length change is characterized by a linear expansion up to –3°C and leads then to a shortening of the sample, which ends in a peak minimum at 8°C. The following slight expansion ends at the initial length of the samples. Thus, no residual strain occurs after the loading cycle. Furthermore, the behaviour for both sample directions of the Velpke sandstone is similar, and therefore no significant directional dependence is detectable. The described length change Type A is observable for the sandstones from Velpke, Bentheim and Ostlutter (Table 6).

The sandstone from Ruethen also shows a linear contraction during cooling and an expansion of sample length below –2°C, with a maximum at about –7°C (Fig. 15e). Subsequently, an extreme contraction that leads to a strong contraction well below the length of the dry sample occurs up to –12°C. This behaviour is different in other rock directions and results in a strong anisotropic length change. The contraction of the wet Ruethen samples is similar to the dry sample condition between –12 and –20°C (Fig. 15f). This linear length change is also observable at the heating stage between –20 and –2°C. Subsequently, both samples show a strong expansion up to 3°C that is followed by a shortening that reaches its maximum at 7°C. The subsequent expansion stage results in a curve fitting to the initial sample length. The length change Type B described here is observable for most of the investigated rocks. Remarkable is that these rocks are characterized by a relatively high content of clay minerals but also of smaller capillary pores and micro-pores.

No significant residual strain occurs for both length change types at capillary water saturation. Thus, no

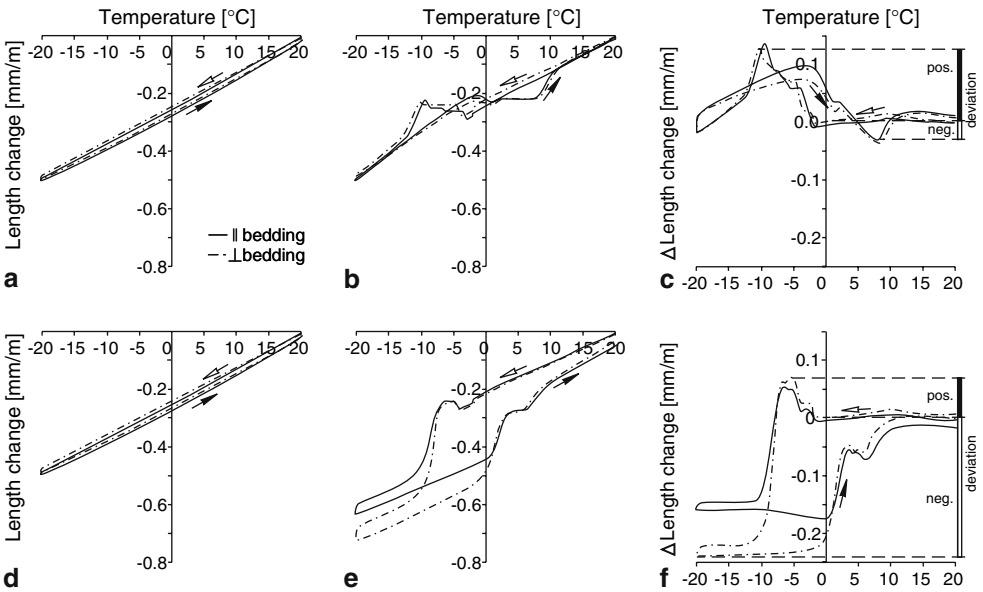

Fig. 15 Different length change patterns during frost loading, exemplarily shown for the **a–c** Velpke (Type A) and **d–f** Ruethen sandstone (Type B): **a**, **d** length change behaviour of dry and **b**, **e** of capillary water-saturated samples as well as **c**, **f** the respective length change difference diagrams

direct deterioration results during the freeze/thaw loading. However, the ice crystallisation clearly affects the samples in terms of stresses which are transmitted to the rock fabric. The maximum deviations from the dry samples length change should be a measure for the stresses that will affect the stone. The positive, negative, and total deviation from the dry sample length change is exemplarily shown in Fig. 15c, f for the sandstones from Velpke and Ruethen. The respective deviations of the rocks investigated differ in a wide range (Table 6). The smallest total deviation values are observable for samples that show the length change pattern Type A, whereas the highest values are in the positive range. In contrast, samples with Type B length change are characterized by a large total deviation and were dominated by negative deviation values.

For better comparison, it is advantageous to divide the length change curves in four zones. This is shown in Fig. 16 for the cooling path of the water-saturated sample from Velpke and Schoetmar. The length change in Zone I is comparable to that of the dry sample condition. This means that water in the pore space has no significant influence on the length change above the freezing point. In Zone II the pronounced expansion can be observed. This expansion can be traced back to ice crystallisation within the pore space of the rock sample. In Zone III a strong contraction occurs. This behaviour is probably caused by a pressure solution (and recrystallisation) of existing ice crystals. In most cases, the contraction of the sample in Zone IV is stronger compared with the behaviour in the dry condition. This can be traced back to the high thermal expansion coefficient of ice.

Measurements were done on samples with varying water content in order to gather information on the length change as a function of the saturation degree. The samples were filled with water by vacuum and then dried to the respective saturation degree. The results are exemplarily shown in Fig. 17 for the Ruethen sandstone with 20, 50, 70, and 80% water content in the pore space. The Ruethen sample shows that a water content of 20% already has an influence on the length change by ice crystallisation (Fig. 17a). The influence increases between 20 and 50% water content (Fig. 17b) and shows a scenario similar to that described for the length change behaviour of the capillary water-saturated sample in Fig. 15e. A pattern change occurs in the test with an 80% saturation degree. The previously observable pronounced contraction at around –7°C changes into a slight sample shortening with a following expansion below –10°C (marked in Fig. 17d as Zone IIIb). This second expansion results in a pronounced residual strain after reaching the initial temperature of 20°C. Thus, the Ruethen sample sustains first deterioration around a saturation degree of 80%. Remarkable is that the second expansion in Zone IIIb, which is surely caused by ice crystallisation, takes place in a relative low temperature range between –8 and –11°C. At this temperature, only water in smaller capillary or micro pores is still unfrozen. Thus, the damage results from ice crystallisation in smaller pores. For extremely high degrees of saturation, large residual strains occur. This is shown in Fig. 18a for the Bad Bentheim sandstone at a saturation degree of 90%. After the loading, the sample shows a residual strain of 1.2 mm/m. The loaded sample is also macroscopically strongly affected (Fig. 18b).

In addition, the effect of the cooling rate of super cooling on the length change induced by ice crystallisation was also investigated. The results are shown for the Ruethen sandstone in Fig. 19. The cooling rates vary from 0.05 to 0.50°C/min. The tests were carried out on capillary water-saturated samples. The maximum expansion below the freezing point occurs for the Ruethen sample when using the 0.50°C/min cooling rate at about –4°C. In contrast, the above mentioned effect does not appear until –7°C when the cooling rate is 0.50°C/min (Fig. 19). Further, the absolute length

Table 6 Positive, negative, and total deviation of length change between dry and wet sample conditions induced by ice crystallisation (*Z*-direction)

Sandstone type	Length change type	Positive deviation (mm/m)	Negative deviation (mm/m)	Total deviation (mm/m)
Cotta	B	0.07	–0.09	0.16
Ruethen	B	0.07	–0.25	0.32
Bentheim	A	0.12	–0.02	0.14
Velpke	A	0.15	–0.04	0.19
Ostlutter	A	0.20	–0.01	0.21
Obernkirchen	B	0.06	–0.13	0.19
Hockeln	B	0.05	–0.12	0.17
Heersum	B	0.03	–0.52	0.55
Ibbenbueren	B	0.05	–0.22	0.27
Schoetmar	B	0.07	–0.71	0.78
Karlshafen	B	0.05	–0.50	0.55
Barkhausen	B	0.09	–0.16	0.25

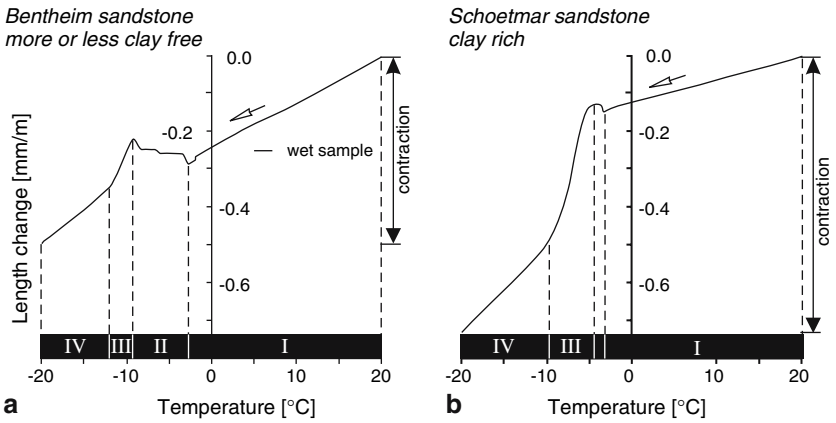

Fig. 16 Zones of length changes during frost loading for **a** the more or less clay free Bentheim and **b** the clay rich Schoetmar sandstone (for explanations see text)

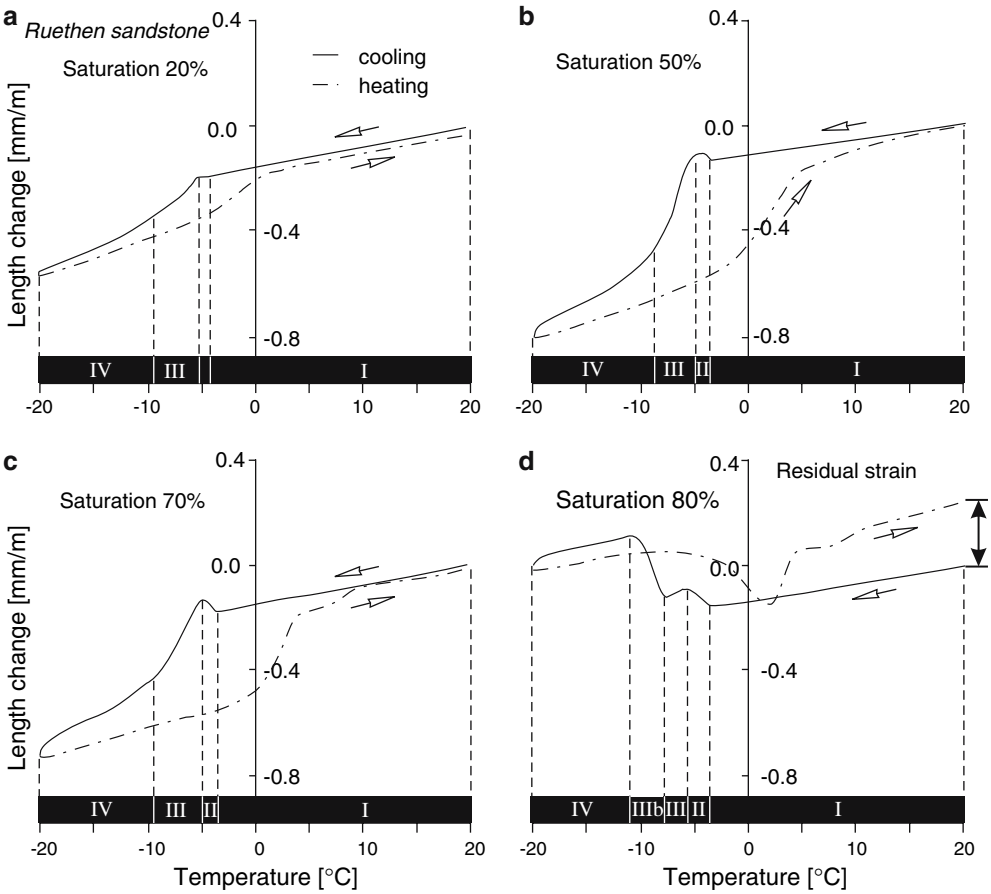

Fig. 17 Influence of the saturation degree on the length change behaviour during frost loading, exemplarily shown for a sample from Ruethen sandstone (the respective water saturation degree is marked in the diagrams)

change varies, whereas the slowly cooled sample exhibits the highest absolute length change. A total length change of 0.7 mm/m can be observed in the *Z*-direction of the Ruethen sample by cooling down from 20 to –20°C at a cooling rate of 0.05°C/min. In contrast, the length change is about 0.6 mm/m when using a cooling rate of 0.50°C/min. Moreover, the hysteresis is much smaller if the samples are cooled down slowly (Fig. 19). Thus, the general length change pattern remains unaffected by the cooling rates used, whereas the temperatures at which the dilatation phenomena takes place, the absolute length changes, and the intensity of hysteresis are different.

The analyses of the temperature show for all samples in wet condition thermal effects during crystallisation and melting. The temperature within the specimen (Dummy temperature) shows a maximum deviation up to 3°C from the linear cooling path.

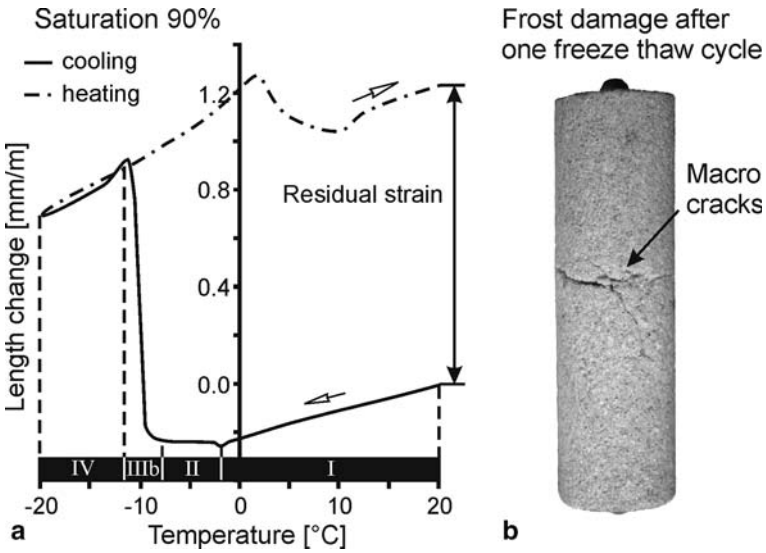

Fig. 18 Strong deterioration of a Bentheim sample at 90% water saturation degree induced by frost action: **a** length change diagram shows a strong expansion around –10°C (Zone IIIb) which results in a large residual strain and **b** damages of the sample after the test

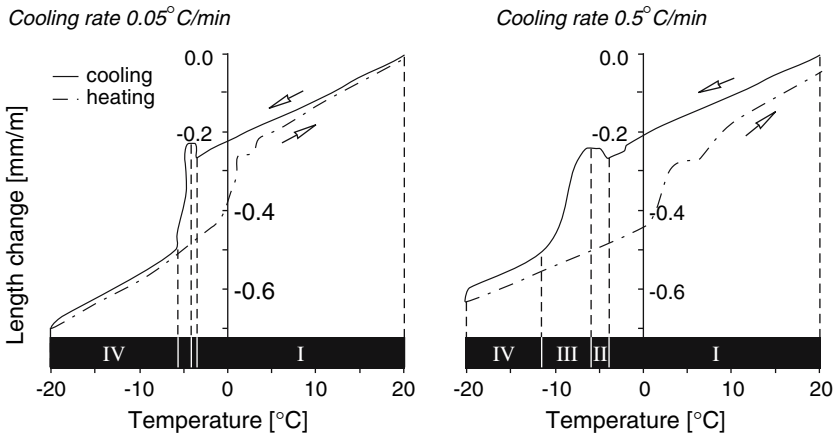

Fig. 19 Influence of the cooling rate on the length change behaviour during frost loading, exemplarily shown for the Ruethen sandstone: cooling rates of **a** 0.05°C/min and **b** 0.50°C/min

However, there is no influence on the length change of the samples. This can be traced back to a limited transfer of the freezing and melting heat to the rock fabric. Based on this, the length change in Figs. 15, 16, 17, 18, 19 is plotted against the chamber temperature.

Discussion

The pore space of sandstones is a major parameter of salt weathering because that is where the crystallisation takes place. The main pore space properties are the effective porosity, the distribution of the pore sizes, the pore shapes, and the pores' interconnection. As far as the sandstones themselves are considered, the controlling elements are the mineralogical composition and the fabric, the later having developed from the original clastic material deposited and the diagenetic evolution (e.g. compaction and cementation). The material's characteristics also determine the petrophysical properties of the rock (Siegesmund 1996). For example, the porosity of sandstones mainly controls the mechanical and elastic properties like tensile strength and ultrasonic velocities, whereas the water transport properties depend on the pore size distribution.

In order to examine the resistibility against salt attacks, conventional salt crystallisation tests were applied that are similar to the ones used in civil engineering. Since the preconditions of these tests are the same, the samples' differing resistibilities can be traced back to the mineralogical composition and the rock fabric. The results of the salt crystallisation tests presented in this article show that the porosity of the sandstones can be considered a major critical weathering parameter. Sandstones with a low porosity can go through more loading cycles than samples that have a high porosity. It is assumed that highly porous rocks

absorb a larger amount of salt solution. Consequently, more salt would crystallise in the pore spaces. Therefore, stronger stresses could develop in the rock fabric. However, highly porous sandstones also exhibit a lower tensile strength and are less resistant to the stresses the salt crystallisation evokes. Evidently, the induced forces have to exceed the tensile strength in order for the damage to occur.

The distribution of the pore size is another crucial rock parameter that critically affects the weathering resistibility of sandstones (Fitzner and Snethlage 1982). Sandstones that had a narrow pore radii distribution and lacked micro-pores (Type A) proved to be particularly resistant. Such pore radii distributions are typical of those sandstones that have a good sorting of detrital components. Geologically speaking, these are predominantly sandstones that have developed as beach sands in a marine environment. Sandstones with a wide range of pore sizes (Type B) or even a bimodal distribution (Type C) did not prove to be particularly resistant to salt corrosion and tended to depend on their porosity.

The rock fabric was also responsible for the particular forms of weathering that the cyclic-loaded sandstone samples visibly showed. The reason is that due to the different behaviour during the drying, the amount of salt increased in various areas of the rock. One of the parameters to determine the dryness of the sandstones is the content of critical moisture (w_{crit}/w_{vac}-value). The w_{crit}/w_{vac}-value is controlled by the pore radii distribution. A large amount of micro-pores or smaller capillary pores leads to higher critical moisture content. The investigations proved that the weathering forms found on the sandstones, which had high contents of critical moisture because of slow drying, was predominantly scaling. It is assumed that slow drying leads to salt enrichment in the deeper areas of the rock. In contrast to that, fast-drying samples are characterized by a granular disintegration at the rock surface, which results from salt enrichment in areas close to the surface.

The way the salt crystals had developed and been distributed in the pore spaces of the sandstones gave evidence that the salt did not occur in the form of a few individual large crystals, but rather as a lot of crystals that settled at the entire internal surface of the rocks. On the one hand, this phenomenon is caused by the right amount of nuclei needed for the crystallisation (cf. Snethlage 1984). On the other hand, it shows that there were no large crystals that could have created stress development in larger capillary pores. The stress development must have had taken place in smaller pores or in pore channels. Thus, sandstones that have large capillary pores and lack micro-pores were expected to sustain a higher salt content for the fabric to deteriorate. The results of the modified salt crystallisation test supported these considerations. The samples that had larger pores and a narrow-spaced Type A pore radii distribution (Bentheim and Velpke) sustained much more salt until damage became effective. In contrast to that, the samples from Cotta and Ruethen exhibited strong deterioration at relatively low salt contents.

The salt crystallisation tests allow general conclusions regarding the relative weathering resistibility of sandstones but provide only limited information about the actual damaging mechanisms. However, other investigation methods such as measuring the length change during the salt loading give more details and help to understand the weathering process much better.

According to the data on the length change, the respective rocks varied in their responses to the salt loading. Whereas the sandstone from Schoetmar exhibited strong residual strain after the cyclic loading, the Ruethen sandstone was more or less unaffected. Unlike the Schoetmar sandstone, the Ruethen sandstone had even contracted. A concluding explanation for the distinct and residual contraction remains unknown. However, it seems questionable that there was a stress-induced fabric collapse due to salt crystallisation, like Kirchner and Worch (1993) suggest. The contraction of the samples indicates that tensile stresses occurred within the fabric, which might have resulted from the dehydration of mirabilite to thenardite.

The salt weathering of the Cotta sandstone showed a strong directional dependency. With respect to the sample that was directed perpendicular to the bedding, the dilatation behaviour was comparable to the Schoetmar sandstone. The sample having an orientation parallel to the *X*-direction illustrated that the Cotta sandstone contracted continuously, which is comparable to the length change behaviour of the Ruethen sandstone. This observed anisotropic behaviour can most probably be attributed to the shape-preferred orientation of the clastic quartz grains, which also produces a shape-preferred orientation of the pore geometry.

The length change behaviour, especially in subsequent loading cycles, indicates that the main deterioration process of sodium sulphate must be hydration. The differences were best observed in both sample directions of the Schoetmar sandstone (Fig. 13). Strong dilatation occurred at the solution up-taking stage of sodium sulphate, which was more than three times as high as in the initial cycle and thus as the original

hygric expansion. Most likely, the strong expansion was determined by the hydration of the water-free salt phase, thenardite. At the beginning of the drying stage, further expansion was observed, which probably resulted from the crystallisation of mirabilite. After this dilatation the samples contracted noticeably, which indicates that the water-free sodium sulphate phase, thenardite, had developed.

The conventional freeze/thaw tests applied provide only limited information about how the ice crystallisation in the pore spaces affects the weathering of sandstones. It was observed that the application of the tests might activate the rock's weak spots made up of rock discontinuities such as partially open microcracks. These observations agree with the results other authors have published (cf. Nicholson and Nicholson 2000). Regarding the sandstones that did not have such flaws, there was no noticeable damage after 100 freeze/thaw cycles, neither visibly nor by means of ultrasonic wave velocities. Thus, the cyclic frost loading at normal water saturation could have led only to long-term deterioration. The frost tests are time consuming and do not provide sufficient information about the weathering resistibility of the material and about the active mechanisms.

Unlike the frost tests, the length change investigations that were carried out during the ice crystallisation in the pore space contain a lot of details about the deterioration mechanisms and help to understand the process of ice-weathering. Water that froze inside of the sandstones' pore spaces resulted in a modification of their length change behaviour. This proved that stresses were induced within the rock. The pattern of the length change curves, which were generated by the ice crystallisation, allows conclusions about the effective mechanisms as well as their dependence on the mineralogical composition and the rock fabric.

Above the freezing point the length change of the wet samples was similar to the one of the dry samples (Zone I). This means that the liquid in the pore space had no influence on the length change in the positive temperature range. Due to the pronounced expansion below the freezing point, a state of ice crystallisation was determined (Zone II). In comparison with the length change behaviour of dry samples, this relative expansion proves that there was stress development in the rock fabric. However, the expansion in Zone II provided no information about the effective mechanism of stress development, i.e. the linear growth pressure or pure volume expansion. It is not likely that volume expansion was responsible for the stress development because the samples were only about 70% saturated with water. Therefore, there was enough vacant pore space for the volume expansion during the phase change from water to ice.

The sample contraction observed in Zone III give more details supporting the model of linear growth pressure as being the major mechanism of stress development. The contraction behaviour can be explained by the pressure solution on the existing ice crystals, which had been under pressure before and were responsible for the expansion in Zone II. The model of linear growth pressure explains that stress develops because of a thin fluid film between the growing ice crystal and the pore surface, which is surrounded by areas with super-cooled water (Scherer 1999). How the pressure in the rock fabric develops depends on the rate of super-cooling of the water. Progressive cooling reduces the amount of the surrounding water because of crystallisation. Thus, the induced stresses are expected to decrease. If the super-cooled water is used up and the thin fluid film is still there, the ice crystal's size can decrease by means of the pressure solution. The result would be a sample shorting, which is what the length change measurements demonstrated in Zone III.

In Zone III there was a pronounced contraction with respect to the sandstones that contained advanced clay minerals. This shorting exceeded the observed expansion induced by ice crystallisation and, thus, cannot be explained only by the pressure solution of the existing ice crystals. All the samples that showed a contraction this strong were characterized by hygric swelling. Thus, a possible mechanism is the decrease of hygric swelling during freezing. Water that is inside of the micro-pores can take higher super-cooling before it crystallises. The unfrozen water in the micro-pores between the clay aggregates or, moreover, intermediate layers of swelling clay minerals could migrate to ice crystals in the larger pores. The swelling pressure of clay minerals could decrease, which would result in a sample shortening. Another explanation, as was introduced by Stockhausen (1981), is the development of a negative pressure in micro-pores. Accordingly, growing ice crystals in larger pores could have sealed the smaller pores, severing the connection to the other pores. The residual water has the ability to migrate to the surrounding ice crystals, which would result in negative pressure within the micro-pores (cf. Weiss 1992).

Compared to the sample behaviour in dry condition, the length change in Zone IV also demonstrated a stronger contraction of the sandstones. This phenomenon can be attributed to the high thermal expansion coefficient of ice. Ice has an $\alpha = 63 \times 10^{-6}\ K^{-1} \parallel c$-axis and $\alpha = 46 \times 10^{-6}\ K^{-1} \perp c$-axis between –20 and –10°C (La Plaza and Post 1960), whereas quartz, the pre-

dominant mineral of the investigated sandstones, has an $\alpha = 9 \times 10^{-6}$ K^{-1} || *c*-axis and $\alpha = 14 \times 10^{-6}$ K^{-1} ⊥ *c*-axis (Skinner 1966). However, the ice crystals have to cohere with the rock grains in order to make the different thermal expansion properties cause the transmission of stresses in the rock fabric. Thus, if the model of linear growth pressure as discussed above is appropriate, the thin liquid film between the ice crystal and the pore surface will have to be completely used up in the temperature range of Zone IV.

It can be assumed that various mechanisms are responsible for the stress that develops at high water saturation degrees and results in the deterioration of the fabric. Since the water saturation seems to be too low to make the pure volume change result in pressure during the transition from water to ice, the stresses developing at low water saturation degrees could be explained by the linear growth pressure. However, the sample deterioration at high water saturation degrees, which could be traced back to the strong expansion in Zone IIIb, might have been caused by the pure volume expansion of ice. The high saturation degree of smaller capillary pores could have been responsible for this behaviour. For that reason the conditioning of the samples to be investigated was important. The applied vacuum saturation completely filled all the accessible pores. When dried to the respective saturation degree, the water of the larger capillary pores evaporated first because the smaller capillary pores showed a higher capillary attraction than the larger ones. Therefore, the smaller capillary pores were supposed to be almost completely filled with water at saturation degrees of about 80%. The volume expansion that took place while the water of those pores was in the process of freezing would then be responsible for the observable deterioration of the samples. However, similarly high water saturation degrees of the smaller capillary pores can also be reached by exposing the building to long-term moisture.

The length change behaviour of wet sandstones when exposed to frost loading strongly depended on the degree of water saturation. Even at very low saturation degrees of 20% the crystallizing ice highly influenced the length change. After returning to the initial temperature, no residual strain and thus no damage occurred when the water saturation was below a certain degree. However, the stresses that developed during the ice crystallisation could lead to long-term deterioration. The investigated sandstones showed a residual strain in one loading cycle when exposed to higher saturation degrees in the range between 70 and 80%, which proved fabric deterioration. There was no damage to the investigated samples at volunteer capillary saturation, which indicates that they were not susceptible to freezing. This corresponds to the results of the conventional freeze/thaw test. However, there was some damage found on frost-sensitive tuffs, which were analyzed in a different, comparable project, at capillary water saturation. Thus, the length change investigations presented could also be used to determine the building stone's resistibility to weathering. The advantage of the method presented is its simple and fast practicability.

Conclusions

The investigations of the physical weathering process caused by crystallizing salt and ice in the sandstones' pore spaces demonstrate that the material properties have a crucial influence on the deterioration behaviour. The mineralogical composition as well as the specific fabric determine the sandstones' physical properties. Based on this fact, it is not just one individual element that is responsible for the weathering sensibility of rock. Evidently, various material properties interact during the weathering process.

Although substantial knowledge has already been gained of the damaging principle of salt and ice crystallisation in general, the actual damaging mechanisms examined on-site are still under discussion. Without a doubt, the complex condition of the building as well as the variety of the processes interacting can be held responsible for that. However, the lacking knowledge results in the impossibility to reliably predict the quantitative effects of the damage in process. This has considerable practical consequences: building stones have been used that do not suit the particular application. In addition to that, for the preservation of historic buildings and monuments, the access to material that is appropriate to the respective weathering conditions existing on-site is limited.

In order to obtain a better understanding of the weathering processes by salt and crystallisation, more interdisciplinary research is needed. The possibility to forecast the damaging mechanisms would lead to an increasing durability of the building's natural stones. Moreover, the preservation of historic buildings would benefit from better judgments how to prevent the stone from deteriorating.

Acknowledgments We are grateful to Dirk Kirchner and Madlen Seidel for their help with the salt crystallisation tests. Thanks go to M Steiger for his comments. Our work was supported by the Deutsche Bundesstiftung Umwelt and the Deutsche Forschungsgemeinschaft (Si 438/17-1/2).

References

Arnold A, Zehnder K (1990) Salt weathering on monuments. In: Advanced workshop analytical methodologies for the investigation of damaged stones, 14–21 September 1990, Pavia (Italy)

Birch F (1960) The velocity of compressional waves in rocks up to 10 kilobars, Part I. J Geophys Res 65:1083–1102

Birch F (1961) The velocity of compressional waves in rocks to 10 kilobars, Part II. J Geophys Res 66:2199–2224

Brakel J van, Modry S, Svata M (1981) Mercury porosimetry: state of the art. Powder Technol 29:1–12

Charola AE, Weber J (1992) The hydration/dehydration mechanisms of sodium sulphate. In: Delgado Rodrigues J (ed) Seventh international congress on the deterioration and conservation of stone. Lisbon, pp 581–590

Charola AE (2000) Salts in the deterioration of porous materials: an overview. J Am Inst Conserv 39:327–343

Chatterji S, Christensen P, Overgaard G (1979) Mechanisms of breakdown of natural stones caused by sodium salts. In: Badan B (ed) Third international congress on the deterioration and conservation of stone. Padova, pp 131–134

Correns CW, Steinborn W (1939) Über die Erklärung der sogenannten Kristallisationskraft. Zeitschrift für Kristallographie 101:117–133

Correns CW (1949) Growth and dissolution of crystals under linear pressure. Discuss Faraday Soc 5:267–71

Darwin CR (1839) Journal of researches into the natural history and geology of the countries visited during the voyage of HMS Beagle round the world. D. Appleton, New York

Doehne E (1994) In situ dynamics of sodium sulfate hydration and dehydration in stone pores: observations at high magnification using the environmental scanning electron microscope. In: Fassina V, Ott H, Zezza F (eds) The conservation of monuments in the Mediterrane Basin. Venice, pp 143–150

Doehne E (2002) Salt weathering: a selective review. In: Siegesmund S, Weiss T, Vollbrecht A (eds) Natural stones, weathering phenomena, conservation strategies and case studies. Geol Soc Spec Publ 205:43–56

Duttlinger W, Knöfel D (1993) Salzkristallisation und Salzschadensmechanismen. Jahresbericht Steinzerfall—Steinkonservierung 1991, Ernst & Sohn Verlag, pp 197–213

Everett DM (1961) The thermodynamics of frost damage to porous solids. Trans Faraday Soc 57:2205–2211

Fitzner B (1969) Die Prüfung der Frostbeständigkeit von Naturbausteinen. Geologische Mitteilungen 10:205–296

Fitzner B, Snethlage R (1982) Einfluß der Porenradienverteilung auf das Verwitterungsverhalten ausgewählter Sandsteine. Bautenschutz und Bausanierung 3–1982:97–103

Hirschwald J (1908) Die Prüfung der natürlichen Bausteine auf ihre Verwitterungsbeständigkeit. Wilhelm Ernst & Sohn, Berlin

Kirchner D, Worch A (1993) Physikalische Vorgänge bei der Salzkristallisation. Bautenschutz und Bausanierung 16:101–103

Kiseleva OA, Kladko SN, Sobolev VD, Churaev NV (1975) Crystallisation and melting of aqueous solutions in capillaries as a model of a porous body. Colloid J USSR 37:1–37

La Plaza S, Post B (1960) Thermal expansion of ice. Acta Cryst 13:503–505

McMahon DJ, Sandberg P, Folliard K, Mehta PK (1992) Deterioration mechanisms of sodium sulfate. In: Rodriques JD, Hendriques F, Jeremisas FT (eds.) Proceedings of 7th international congress of deterioration and conservation of stone, vol 2. Portugal, Lisbon, pp 705–714

Mortensen H (1933) Die Salzsprengung und ihre Bedeutung für die regionalklimatische Gliederung der Wüsten. Petermann's Mitteilungen aus Justus Perthes geographischer Anstalt 79:130–135

Nicholson DT, Nicholson FH (2000) Physical deterioration of sedimentary rocks subjected to experimental freezing and thawing. Earth Surf Process Landf 25:1295–1307

Powers TC (1945) A working hypothesis for further studies of frost resistance of concrete. J ACI Proc 41:245–272

Powers TC (1949) The air requirement of frost resistant concrete. Proc Highway Res Board V29:184–211

Powers TC (1955) Resistance of concrete tor frost at early ages. In: Proceedings of RILEM symposium on winter concreting, pp 1–47

Price C, Brimblecombe P (1994) Preventing salt damage in porous materials. In: Ashok R, Smith P (eds) Prepr. Contr. Ottawa Congr. Preventive conservation-practice, theory and research IIC, London, pp 90–93

Pühringer J (1983) Salt disintegration: salt migration and degradation by salt—a hypothesis. Swedish Council for Building Research D15, Stockholm

Pühringer J, Engstrom L (1985) Unconventional methods for the prevention of salt damage. In: Furlan V (ed) Proceedings of 5th international congress on deterioration and conservation of stone 1:241–250

Putnis A, Mauthe G (2001) The effect of pore size on cementation in porous rocks. Geofluids 1:37–41

Rodriguez-Navarro C, Doehne E (1999) Salt weathering: influence of evaporation rate, supersaturation and crystallization pattern. Earth Surf Process Landf 24:191–209

Rodriguez-Navarro C, Doehne E, Sebastián E (2000) How does sodium sulfate crystallize? Implications for the decay and testing of building materials. Cement Concr Res 16(3):947–954

Rossi-Manaresi R, Tucci A (1991) Pore structure and the disruptive or cementing effect of salt crystallization in various types of stone. Stud Conserv 36:53–58

Ruedrich J, Kirchner D, Seidel M, Siegesmund S (2005) Deterioration of natural building stones induced by salt and ice crystallisation in the pore space as well as hygric expansion processes. In: Siegesmund S, Auras M, Ruedrich J, Snethlage R (eds) Geowissenschaften und Denkmalpflege, Zeitschrift Deutsche Geologische Gesellschaft 156/1:59–73

Scherer GW (1999) Crystallization in pores. Cement Concr Res 29:1347–1358

Siegesmund S (1996) The significance of rock fabrics for the geological interpretation of geophysical anisotropies. Geotektonische Forschung 85:1–123

Skinner BJ (1966) Thermal expansion. In: Clark SP (ed) Handbook of physical constants. Geol Soc Am 97:75–96

Snethlage R (1984) Steinkonservierung. Bayerisches Landesamt für Denkmalpflege. Arbeitshefte 22:203

Snethlage R, Wendler E (1997) Moisture cycles and sandstone degradation. In: Baer NS, Snethlage R (eds) Saving our architectural heritage. The conservation of historic stone structures. Elsevier, Chichester, pp 7–24

Sperling CHB, Cooke RU (1980) Salt weathering in arid environments. I. Theoretical considerations. Bedford Coll Pap Geogr 9:52

Steiger M, Dannecker W (1998) Die Bedingungen für die Kristallisation verschiedener Salzhydrate am Beispiel Thenardit/Mirabilit. In: Jahresberichte Steinzerfall-Steinkonservierung, Band 6, 1994–1996. Frauenhofer IRB Verlag, Stuttgart, pp 123–133

Steiger M, Neumann HH, Grodten T, Wittenburg C, Dannecker W (1998) Salze in Natursteinmauerwerk: Probenahme, Messung und Interpretation. In: Snethlage R (ed) Natursteinkonservierung 2. Fraunhofer IRB Verlag, Stuttgart, pp 61–91

Steiger M (2005) Crystal growth in porous materials. I: The crystallisation pressure of large crystals. J Cryst Growth 282:455–469

Stockhausen N (1981) Die Dilatation hochporöser Festkörper bei Wasseraufnahme und Eisbildung. Ph.D. TU München, pp 163

Sunagawa I (1981) Characteristics of crystal growth in nature as seen from the morphology of mineral crystals. Bull Mineral 104:81–87

Taber S (1916) The growth of crystals under external pressure. Am J Sci 41:532–556

Weiss G (1992) Die Eis und Salzkristallisation im Porenraum von Sandsteinen und ihre Auswirkung auf das Gefüge unter besonderer Berücksichtigung gesteinsspezifischer Parameter. Münchner Geowissenschaftliche Abhandlungen B 9:62

Wellman HW, Wilson AT (1965) Salt weathering, neglected geological erosive agent in coastal and arid environments. Nature 205:1097–1098

Wellman HW, Wilson AT (1968) Salt weathering or fretting. In: Fairbridge RW (eds) The encyclopedia of geomorphology. Stroudsburg, Pennsylvania

Winkler EM (1968) Frost damage to stone and concrete: geological considerations. Eng Geol 2:315–323

Winkler EM, Wilhelm EJ (1970) Salt burst by hydration pressures in architectural stone in urban atmosphere. Bull Geol Soc Am 81:567–572

Winkler EM (1975) Stone: properties, durability in man's environment, 2nd edn. Springer, Vienna, New York

Winkler EM (1994) Stone in architecture, 3rd edn. Springer, Berlin Heidelberg New York

Zehnder K, Arnold A (1989) Crystal growth in salt efflorescence. J Cryst Growth 97:513–521